Experiments on two-layer density-stratified inertial gravity currents

Albert Dai[*]

Department of Engineering Science and Ocean Engineering, National Taiwan University,
Taipei 10617, Taiwan

Experiments for the gravity currents produced from a two-layer density-stratified buoyancy source in a full-depth, lock-exchange setup with a scaling analysis describing the flow morphologies are presented. In the inertial phase of propagation, the 3/2 power relationship $x_f^{3/2} = 1.5 F_I B_0^{1/2} (t + t_I)$ robustly applies between the front location x_f and time t, where F_I is the Froude number in the inertial phase, B_0 is the total released buoyancy, and t_I is the t-intercept. We showed that the Froude number in the inertial phase is not a universal constant but depends on the two controlling parameters, namely, the density difference ratio, $R_\rho = (\rho_U - \rho_0)/(\rho_L - \rho_0)$, where ρ_U, ρ_L, and ρ_0 are the densities of the fluids in the upper layer, lower layer, and ambient environment, respectively, and the buoyancy distribution parameter, $R_B = B_U/B_0$, where B_U is the buoyancy in the upper layer. For a given buoyancy distribution parameter, the Froude number in the inertial phase decreases monotonically as the density difference ratio decreases. For a given density difference ratio, the Froude number in the inertial phase has a local minimum as the buoyancy distribution parameter falls in the range of $0.3 \lesssim R_B \lesssim 0.5$. When the buoyancy source is homogeneous, the Froude number in the inertial phase has its maximum value at $F_I = 1.33 \pm 0.02$. The flow morphology is also found to depend on the two controlling parameters. For weakly stratified two-layer heavy fluid, $0.4 \lesssim R_\rho < 1$, mixing between the fluids from the two layers is more immediate. For strongly stratified two-layer heavy fluid, $0 < R_\rho \lesssim 0.4$, there is less mixing between the layers for flows dominated by the upper layer, $R_B \to 1$, and for flows dominated by the lower layer, $R_B \to 0$. For gravity currents that are produced from a strongly stratified source and dominated by the upper layer, the upper layer may override and outrun the lower layer, which initially takes the lead after the two-layer heavy fluid is released. For gravity currents that are produced from a strongly stratified source and dominated by the lower layer, the lower layer may outrun the upper layer from the outset, resulting in streamwise stratification. Surprisingly, for the gravity currents produced from a strongly stratified source, mixing of fluids from the two layers can be enhanced when the buoyancy distribution parameter falls in the range of $0.3 \lesssim R_B \lesssim 0.5$. Such an exceptional observation is now successfully explained by the scaling analysis.

I. INTRODUCTION

Gravity currents, also known as density currents, occur when fluid of one density propagates along a horizontal boundary into fluid of a different density. In geological and engineering environments, the density difference can be attributed to a number of factors, including temperature differentials, dissolved materials, and suspended sediments. Readers are referred to Refs. [1–4] for a comprehensive introduction to this topic and review of the examples.

Gravity currents have been studied extensively in laboratory experiments since the 1950s. These experiments of gravity currents have been typically performed in a closed, rectangular cross section and horizontal channel with a vertical barrier, where two sides of the barrier are filled with fluids

---

[*]hdai@ntu.edu.tw

073802-1

of different densities. Removal of the barrier then sets the two fluids into motion. This type of experiment, lock-exchange setup, serves as a paradigm configuration for studying the evolution of gravity currents [5–12]. Other related studies include the influence of the cross section on the propagation of gravity currents by lock exchange, which has been addressed by Ref. [13], and the influence of favorable and adverse slopes, which has been investigated by Refs. [14–23].

It is well known that gravity currents produced by lock exchange may go through three different phases of spreading in sequence, namely, the slumping, inertial, and viscous phases. In the slumping phase, the speed of the gravity current front is nearly constant (within experimental error). The speed of the front, U_f, in the slumping phase can be expressed in terms of the reduced gravity, $g'_0 = g(\rho_C - \rho_0)/\rho_0$, depth of channel, H, and Froude number in the slumping phase, F_S, as

$$U_f = F_S \sqrt{g'_0 H}, \tag{1}$$

where ρ_C is the density of homogeneous heavy fluid and ρ_0 is the density of ambient light fluid. For full-depth lock exchange flows, Refs. [24] and [25] found F_S to vary between 0.45 and 0.5 for sufficiently high Reynolds numbers. For energy-conserving gravity currents, as is the case for gravity currents at sufficiently high Reynolds numbers, Refs. [26] and [5] show that $F_S = 0.5$.

In the inertial phase, a balance between the buoyancy and inertial forces is struck and the gravity currents start to decelerate in time following $U_f \sim t^{-1/3}$. The speed of the front in the inertial phase can be expressed as

$$U_f = F_I \sqrt{g'_0 h_f}, \tag{2}$$

where F_I is the Froude number in the inertial phase and h_f is the current height. Reference [27] indicated that in the inertial phase, $F_I \approx 1.19$ when $h_f/H \leqslant 0.075$, while Ref. [26] indicated that $F_I \to \sqrt{2}$ in the limit of $h_f \ll H$. Finally in the viscous phase, when the viscous force balances the buoyancy, the gravity currents decelerate even more rapidly than in the inertial phase. Reference [28] showed that the speed of the front in the viscous phase follows $U_f \sim t^{-4/5}$.

In the literature, our understanding of gravity currents produced by lock exchange is mainly built on flows that develop from initially homogeneous buoyancy sources. A number of previous investigations have been focused on the release of heavy fluid into a density-stratified environment, including Refs. [29–34] for bottom-propagating gravity currents and [35–40] for gravity currents propagating at some intermediate depth in the stratified environment. However, little is known about the gravity currents produced from buoyancy sources that are already density-stratified at the time of release [41]. In reality, the buoyancy sources may become vertically density-stratified in terms of suspended particle size and concentration of dissolved materials due to a number of processes, which include different settling velocities of suspended particles, variations in turbulence intensity within the flow, entrainment of ambient fluid at the margins, and entrainment of sediment from the erodible substrate. In many situations, e.g., in the study of deposits of turbidity currents, and pyroclastic flows [42,43], knowledge of the density-stratified gravity currents is helpful in offering possible explanations for observed features of particle segregation [44–46].

The purpose of present investigation is to deepen our understanding of the gravity currents produced from a buoyancy source which is already density-stratified at the time of release. Our focus in this study is on the inertial phase of propagation and the buoyancy source is simplified as a two-layer heavy fluid. The investigation is conducted systematically by varying the depths and densities of fluids in the two layers, while the average density of the two-layer system is maintained unchanged in all experiments. The objective is to investigate qualitatively and quantitatively how the inertial gravity currents are influenced by the two controlling parameters, namely the density difference ratio and the buoyancy distribution parameter, which will be introduced in the following section. Although Ref. [47] performed a similar series of experiments to the ones presented here, the spatial-temporal resolution therein was relatively insufficient to quantify the dependence of the Froude number on the density difference ratio and the buoyancy distribution parameter. In Sec. II, we
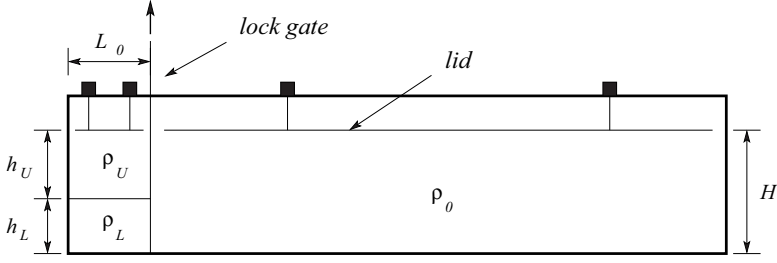
FIG. 1. Side view of the channel used in the experiments for gravity currents produced from a two-layer density-stratified buoyancy source. The ambient is filled with fluid of density ρ_0, and the heavy fluid region consists of two layers, where the lower layer is filled with fluid of density ρ_L and thickness h_L and the upper layer is filled with fluid of density ρ_U and thickness h_U. The depth of the ambient is equal to the total depth of the heavy fluid region and is maintained at $H = 20$ cm in the experiments. The lock gate is placed at a constant distance $L_0 = 10$ cm from the left wall. The channel is fitted with a rigid lid to make the boundary conditions identical at the top and bottom of the channel. Removal of the gate then sets the two-layer heavy fluid into motion.

summarize the 3/2 power relationship for the front location history in the inertial phase and present a scaling analysis, which describes the mixing and separation processes involved in the evolution of gravity currents. The experimental procedures are described in Sec. III, and the qualitative and quantitative results are presented in Sec. IV. Finally, conclusions are drawn in Sec. V.

II. THEORETICAL BACKGROUND

The configuration of the problem is sketched in Fig. 1. The two-layer density-stratified heavy fluid is placed on the left hand side of the lock gate, while the ambient light fluid is placed on the other side. After the lock gate is removed, the heavy fluid collapses out of the lock region. Since the lock length is short compared with the length of the channel, the gravity currents accelerate for a short period and quickly move into a state, the inertial phase, where a balance of inertial and buoyancy forces is struck and the viscous force is considered to be unimportant.

In the inertial phase, the two-dimensional initial buoyancy per unit width

$$B_0 = g_0' H L_0 \quad \text{where} \quad g_0' = \frac{\rho_C - \rho_0}{\rho_0} g \tag{3}$$

is a parameter that must be considered. Here H and L_0 are the initial height and length of the lock, respectively, and ρ_C and ρ_0 are the average density of the two-layer heavy fluid and density of ambient fluid, respectively. The average density of the two-layer heavy fluid is defined by

$$\rho_C = \rho_L \frac{h_L}{H} + \rho_U \frac{h_U}{H}, \tag{4}$$

where ρ_L and ρ_U denote the densities of fluids in the lower and upper layers, respectively, and h_L and h_U denote the thicknesses of the lower and upper layers, respectively. At the time of release, the initial potential energy per unit width is defined as

$$E_{p0} = L_0(\rho_L - \rho_0)g\frac{h_L^2}{2}L_0(\rho_U - \rho_0)gh_U\left(h_L + \frac{h_U}{2}\right), \tag{5}$$

and it should be kept in mind that, although the average density of the two-layer heavy fluid remains unchanged in the experiments, the initial potential energy depends on the initial density distribution between the two layers.

Let the position of the gravity current front be designated as x_f and the time as t, then the front velocity is the time rate of change of x_f, namely, U_f. Following Ref. [27], the Froude number in the

inertial phase at the front is given by

$$F_I = \frac{U_f}{B_0^{1/2} x_f^{-1/2}}.$$ (6)

Using the fact that $U_f = dx_f/dt$, (6) can be integrated with respect to time as

$$x_f^{3/2} = 1.5 F_I B_0^{1/2}(t + t_I),$$ (7)

where t_I is a constant of integration which can be found by identifying the t-intercept in the plot of $x_f^{3/2}$ against t. This relationship has been shown to describe the inertial gravity currents produced from homogeneous and density-stratified buoyancy sources well [47]. For inertial gravity currents produced from a homogeneous buoyancy source, [27] reported that $F_I \approx 1.19$ when $h_f/H \leqslant 0.075$; for those produced from a two-layer density-stratified buoyancy source, Ref. [47] reported that $F_I \approx 1.3$.

In the gravity currents produced from a two-layer density-stratified buoyancy source, the evolution of the gravity currents is mainly controlled by two important processes, which are the mixing and separation between the layers. The gravity currents would become streamwise stratified, i.e., the two layers separate in the streamwise direction, if the layers are unable to mix in the early stage of the flow development. Conversely, the flow would be unable to become streamwise stratified once the two layers mix.

A simple scaling analysis, in the spirit of the analysis by Ref. [47], may help identify the important parameters characterizing the evolving structure of the gravity currents. If the two layers of the initial vertical stratification are considered as propagating forward at different speeds, then the dimensionless time scale for the two layers to separate by a distance L_0 will be

$$\tau_{\text{sep}} \sim \frac{B_0^{1/2}}{\left| B_L^{1/2} - B_U^{1/2} \right|},$$ (8)

where $B_L = g_L' h_L L_0$ and $B_U = g_U' h_U L_0$ represent the buoyancy in the lower layer and the buoyancy in the upper layer, respectively. The lower layer has thickness h_L and reduced gravity $g_L' = g(\rho_L - \rho_0)/\rho_0$; the upper layer has thickness h_U and reduced gravity $g_U' = g(\rho_U - \rho_0)/\rho_0$, as illustrated in Fig. 1. The speeds of propagation of the lower and upper layers are estimated as $B_L^{1/2} L_0^{-1/2}$ and $B_U^{1/2} L_0^{-1/2}$, respectively, and the time scale for nondimensionalization based on the bulk density is $B_0^{-1/2} L_0^{3/2}$.

When the gravity current is dominated either by the upper layer or by the lower layer, $B_U \gg B_L$ or $B_L \gg B_U$, the dimensionless time scale of separation is of order unity, $\tau_{\text{sep}} \approx O(1)$, since $B_0 = B_L + B_U$. However, it is important to note that when $B_L \approx B_U$, according to (8), the dimensionless time scale of separation can become greater than order unity. In this situation the two layers propagate forward at similar speeds maintaining contact without separation for an extended period.

When the two layers mix, the growth rate of the mixed region, nondimensionalized by the velocity scale $B_0^{1/2} L_0^{-1/2}$, is estimated as αRi^{-1} using the entrainment law [48], where α is the entrainment coefficient of order 10^{-1} [48–50] and

$$\text{Ri} \sim \frac{(g_L' - g_U')H}{B_0 L_0^{-1}}$$ (9)

is an estimate for the bulk Richardson number. Supposing that the mixed layer has thickness h_{mix}, the dimensionless time scale for the mixed layer to grow to the thickness h_{mix} is estimated as

$$\tau_{\text{mix}} \sim \frac{1}{\alpha} \frac{g_L' - g_U'}{g_0'} \frac{h_{\text{mix}}}{H}.$$ (10)

During the initial development of the flow, the thickness of the mixed layer is expected to be limited by the smaller of h_L and h_U. As a result, $\tau_{\text{mix}} \to 0$ when $h_{\text{mix}}/H \to 0$, i.e., when either

$h_L/H \to 0$ or $h_U/H \to 0$. Physically, $h_{\mathrm{mix}}/H \to 0$ represents that one of the two layers is extremely thin compared with the other and in this case mixing is immediate. However, such a case is not of particular interest, and, in this study, we shall be concerned with the situation when $h_{\mathrm{mix}}/H \lesssim O(1)$ but $h_{\mathrm{mix}}/H \nrightarrow 0$.

Alternative models describing the entrainment (e.g., Refs. [51,52]) may lead to other functional forms for the dimensionless time scale of mixing than the one presented here. Nevertheless, the scaling analysis essentially describes the mixing and separation processes and explains the different flow morphologies, as will be shown in the following section.

For gravity currents to become streamwise stratified, the dimensionless time scale of separation must be shorter than that of mixing, namely, $\tau_{\mathrm{mix}} \gg \tau_{\mathrm{sep}}$, which leads to $g'_L \gg g'_U$ and provided the dimensionless time scale of separation is not much greater than order unity. If this condition is expressed in terms of the density difference ratio,

$$R_\rho = \frac{\rho_U - \rho_0}{\rho_L - \rho_0}, \tag{11}$$

which is essentially the ratio of the reduced gravity in the upper layer to that in the lower layer, $R_\rho = g'_U/g'_L$, then the necessary condition for gravity currents to be streamwise stratified, namely, $g'_L \gg g'_U$, becomes $R_\rho \ll 1$, which is also termed as a "strongly" stratified source. For gravity currents produced from a strongly stratified source, the flow may be dominated either by the upper layer or by the lower layer, depending on the distribution of buoyancy between the two layers. These differing behaviors can be expressed by the buoyancy distribution parameter defined by

$$R_B = \frac{B_U}{B_0}. \tag{12}$$

When $R_B \to 1$ the flow is dominated by the upper layer, and when $R_B \to 0$ the flow is dominated by the lower layer.

However, according to (8) and (10), the time scale of mixing can still be shorter than that of separation, $\tau_{\mathrm{sep}} > \tau_{\mathrm{mix}}$, even when the buoyancy source is strongly stratified, $R_\rho \ll 1$, provided $B_L \approx B_U$. This exceptional case can lead to enhanced mixing in the gravity currents produced from a strongly stratified source. In essence, the reason for enhanced mixing in this exceptional case lies in the fact that the buoyancy is equally distributed between the two layers, as such the two layers propagate forward at similar speeds. Therefore, the fluids from the two layers keep in contact for an extended period, which allows for enhanced mixing even when the buoyancy source is strongly stratified.

For two arbitrary layers to mix and produce a homogeneous inertial gravity current, the time scale of mixing must always be shorter than that of separation and the condition $R_\rho \to 1$, which is also termed as a "weakly" stratified source, is then required.

III. EXPERIMENTS

A sketch of the experimental setup is shown in Fig. 1. The channel used in the experiments was manufactured with a rectangular cross section 0.2 m wide, 0.3 m deep, and 2.4 m long with transparent Perspex sidewalls. A lock gate was placed at a distance $L_0 = 10$ cm from the left wall. The two-layer density-stratified heavy fluid was carefully filled with a sponge on the left-hand side of the gate, and the ambient light fluid was placed on the right-hand side of the gate. During the experiments, the ambient light fluid was fresh water, and the excess density of the heavy fluid layers was created using sodium chloride. The depth of the two-layer heavy fluid was maintained at $H = 20$ cm. The lower layer thickness and the upper layer thickness were varied systematically in the ranges of $0.085 \leqslant h_L/H \leqslant 1$ and $0 \leqslant h_U/H \leqslant 0.915$ while $h_L + h_U = H$ was maintained throughout the experiments. The depth of the ambient was equal to the total depth of the two-layer heavy fluid. The upper fluid boundary was in contact with two sheets of Perspex, which were

separated by a thin gap to allow the lock gate to be easily removed. Removing the lock gate then sets the two-layer heavy fluid and ambient light fluid into motion.

A uniform LED light board and a light-diffusing screen were placed against the back wall. A Canon 700D camera (1920×1080 pixel resolution at 24 frames per second) was positioned 10 m away from, and normal to, the front wall. The x and y axes in the images align with the horizontal bottom boundary and the wall-normal direction, respectively. The heavy fluid region consisted of two layers of different densities. The lower layer was colored with 5 ml of blue dye per 1 L of solution of sodium chloride, and the upper layer was colored with 6 ml of yellow dye per 1 L of solution of sodium chloride. Blue and yellow colors were chosen to allow the layers to be distinguished and the mixing between the layers, as indicated by the green color, to be clearly visualized. The ambient fluid was not colored and shown as white in the images. The images of gravity currents were recorded and exported into a PC where postprocessing was performed.

Densities of the ambient and heavy fluids were measured using a density meter with an accuracy of 10^{-4} g cm^{-3}. The density of ambient fluid was maintained at $\rho_0 = 0.9955 \pm 0.0016$ g cm^{-3}. In each experiment, the density difference between the heavy and ambient fluids was solely due to dissolved sodium chloride. Slight temperature variations between experimental runs, due to seasonal changes in air temperature, could produce a density change in ambient fluid between runs. However, the density change due to temperature variations was very small compared with that produced by dissolved sodium chloride. The average density of the two-layer density-stratified heavy fluid, defined by (4), was carefully maintained at $\rho_C = 1.0400$ g cm^{-3} throughout the experiments. Therefore, the total amount of sodium chloride dissolved in the heavy fluid was maintained constant. Only the distribution of sodium chloride between the layers was varied to aid comparison of flow behavior. The kinematic viscosity of the sodium chloride solution is taken as $\nu = 1.1 \times 10^{-2}$ cm^2 s^{-1} [53]. Reynolds numbers in the experiments based on the bulk density of the two-layer heavy fluid, $\mathrm{Re} = \sqrt{g_0' H^3}/\nu$, were approximately $\mathrm{Re} \approx 53\,000$, which is far in excess of 1000, above which the inertial phase of propagation could be attained and viscous effects have been thought to be unimportant [3].

IV. RESULTS

In what follows the experimental results for gravity currents produced from a two-layer density-stratified buoyancy source are presented in order. First, we shall present the results for gravity currents produced from a homogeneous buoyancy source, i.e., $R_\rho = 1$. Second, the gravity currents produced from a "weakly" stratified buoyancy source are presented. Third, the gravity currents produced from a "strongly" stratified buoyancy source are presented. In the experiments, by "weakly" we mean that the density difference ratio is in the range of $0.4 \lesssim R_\rho < 1$, in comparison with a "strongly" stratified source in which the density difference ratio is in the range of $0 < R_\rho \lesssim 0.4$. In fact, there is no such a clear distinction between a "weakly" stratified source and a "strongly" stratified one. The classification of two-layer density-stratified buoyancy sources into weakly and strongly stratified ones is based on the observation and at the author's discretion in order to distinguish different flow morphologies between small density contrast and large density contrast in the two-layer heavy fluid system.

Specifically, for weakly stratified two-layer heavy fluid, we shall present the case when the flow is dominated by the lower layer, $R_B \to 0$, and the case when the flow is dominated by the upper layer, $R_B \to 1$. For strongly stratified two-layer heavy fluid, we shall present the case when the flow is dominated by the lower layer, $R_B \to 0$, the case when the flow is dominated by the upper layer, $R_B \to 1$, and the exceptional case when the buoyancy distribution parameter falls in the range of $0.3 \lesssim R_B \lesssim 0.5$.

As there is no clear distinction between weakly and strongly stratified sources, neither is there a clear transition of flow morphology between an upper layer–dominated flow and a lower layer–dominated flow. The cases presented in the paper are selected in order to highlight qualitatively distinct flow morphologies in the parameter space under investigation. The operational parameters, dependent variables, and experimental constants are listed in Table I and Table II. In each

TABLE I. Table showing operational parameters, including the depths of the upper layer and lower layer, h_L/H and h_U/H, average density of the two-layer heavy fluid, ρ_C, densities of fluids in the lower layer and upper layer, ρ_L and ρ_U, density of ambient fluid, ρ_0, and initial potential energy per unit width in the two-layer system, E_{p0}. The unit for the density is g cm^{-3}. The densities of fluids in the lower layer and upper layer are carefully controlled so that the average density of the two-layer heavy fluid is maintained at $\rho_C = 1.0400$ g cm^{-3}. The lock geometry, $H = 20$ cm and $L_0 = 10$ cm, is maintained fixed for all experiments. The initial potential energy per unit width in the two-layer system is in units of 10^4 g cm s^{-2}. Each experimental setup is repeated at least five times. The error estimates are to add and subtract the maximum and minimum values and are not the r.m.s. estimates.

Experiment	h_L/H	h_U/H	ρ_C	ρ_L	ρ_U	ρ_0	E_{p0}
A1	1.000	−	1.0400	1.0400	−	$0.9967^{+0.0001}_{-0.0002}$	$8.4994^{+0.0353}_{-0.0235}$
B1	0.200	0.800	1.0400	1.0450	1.0388	$0.9966^{+0.0003}_{-0.0003}$	$8.3110^{+0.0667}_{-0.0510}$
B2	0.200	0.800	1.0400	1.0500	1.0375	$0.9965^{+0.0001}_{-0.0002}$	$8.1345^{+0.0471}_{-0.0118}$
B3	0.200	0.800	1.0400	1.0550	1.0363	$0.9962^{+0.0001}_{-0.0001}$	$7.9971^{+0.0275}_{-0.0118}$
B4	0.200	0.800	1.0400	1.0600	1.0350	$0.9962^{+0.0001}_{-0.0002}$	$7.8166^{+0.0314}_{-0.0275}$
B5	0.200	0.800	1.0400	1.0650	1.0338	$0.9955^{+0.0001}_{-0.0002}$	$7.7577^{+0.0314}_{-0.0275}$
B6	0.200	0.800	1.0400	1.0700	1.0325	$0.9959^{+0.0002}_{-0.0003}$	$7.4791^{+0.0549}_{-0.0432}$
B7	0.200	0.800	1.0400	1.0750	1.0313	$0.9965^{+0.0001}_{-0.0001}$	$7.1691^{+0.0118}_{-0.0275}$
B8	0.200	0.800	1.0400	1.0800	1.0300	$0.9958^{+0.0003}_{-0.0003}$	$7.0985^{+0.0628}_{-0.0549}$
B9	0.200	0.800	1.0400	1.1050	1.0238	$0.9951^{+0.0006}_{-0.0003}$	$6.2509^{+0.0667}_{-0.1099}$
C1	0.400	0.600	1.0400	1.0450	1.0367	$0.9944^{+0.0009}_{-0.0004}$	$8.5543^{+0.0785}_{-0.1766}$
C2	0.400	0.600	1.0400	1.0500	1.0333	$0.9950^{+0.0003}_{-0.0004}$	$8.0481^{+0.0746}_{-0.0628}$
C3	0.400	0.600	1.0400	1.0550	1.0300	$0.9946^{+0.0006}_{-0.0003}$	$7.7264^{+0.0628}_{-0.1138}$
C4	0.400	0.600	1.0400	1.0600	1.0267	$0.9949^{+0.0006}_{-0.0010}$	$7.2829^{+0.1923}_{-0.1216}$
C5	0.400	0.600	1.0400	1.0650	1.0233	$0.9946^{+0.0006}_{-0.0004}$	$6.9416^{+0.0824}_{-0.1138}$
C6	0.400	0.600	1.0400	1.0700	1.0200	$0.9947^{+0.0006}_{-0.0004}$	$6.5335^{+0.0785}_{-0.1177}$
C7	0.400	0.600	1.0400	1.0750	1.0167	$0.9950^{+0.0003}_{-0.0002}$	$6.0822^{+0.0392}_{-0.0589}$
C8	0.400	0.600	1.0400	1.0800	1.0133	$0.9956^{+0.0001}_{-0.0001}$	$5.5721^{+0.0196}_{-0.0196}$
D1	0.600	0.400	1.0400	1.0450	1.0325	$0.9947^{+0.0007}_{-0.0003}$	$8.3032^{+0.0549}_{-0.1413}$
D2	0.600	0.400	1.0400	1.0500	1.0250	$0.9945^{+0.0003}_{-0.0004}$	$7.7577^{+0.0706}_{-0.0667}$
D3	0.600	0.400	1.0400	1.0550	1.0175	$0.9948^{+0.0004}_{-0.0002}$	$7.0946^{+0.0471}_{-0.0706}$
D4	0.600	0.400	1.0400	1.0600	1.0100	$0.9947^{+0.0015}_{-0.0006}$	$6.5295^{+0.1216}_{-0.2904}$
D5	0.600	0.400	1.0400	1.0420	1.0370	$0.9947^{+0.0006}_{-0.0007}$	$8.6603^{+0.1295}_{-0.1256}$
E1	0.800	0.200	1.0400	1.0450	1.0200	$0.9949^{+0.0001}_{-0.0000}$	$8.0599^{+0.0039}_{-0.0157}$
E2	0.800	0.200	1.0400	1.0420	1.0320	$0.9948^{+0.0004}_{-0.0003}$	$8.5622^{+0.0510}_{-0.0863}$
E3	0.800	0.200	1.0400	1.0410	1.0360	$0.9946^{+0.0002}_{-0.0001}$	$8.7427^{+0.0275}_{-0.0314}$
E4	0.800	0.200	1.0400	1.0460	1.0160	$0.9954^{+0.0001}_{-0.0001}$	$7.8166^{+0.0118}_{-0.0275}$
F1	0.730	0.270	1.0400	1.0505	1.0117	$0.9952^{+0.0001}_{-0.0001}$	$7.2898^{+0.0196}_{-0.0196}$
F2	0.783	0.217	1.0400	1.0468	1.0157	$0.9953^{+0.0002}_{-0.0001}$	$7.7298^{+0.0235}_{-0.0353}$
F3	0.844	0.156	1.0400	1.0430	1.0238	$0.9952^{+0.0001}_{-0.0002}$	$8.2971^{+0.0353}_{-0.0235}$
F4	0.878	0.122	1.0400	1.0411	1.0319	$0.9954^{+0.0002}_{-0.0001}$	$8.5567^{+0.0196}_{-0.0392}$
G1	0.412	0.588	1.0400	1.0715	1.0180	$0.9955^{+0.0002}_{-0.0001}$	$6.1782^{+0.0275}_{-0.0314}$
G2	0.483	0.517	1.0400	1.0603	1.0211	$0.9956^{+0.0001}_{-0.0000}$	$6.7854^{+0.0078}_{-0.0118}$
G3	0.583	0.417	1.0400	1.0490	1.0274	$0.9957^{+0.0002}_{-0.0003}$	$7.6616^{+0.0589}_{-0.0392}$
G4	0.651	0.349	1.0400	1.0434	1.0337	$0.9958^{+0.0001}_{-0.0002}$	$8.2448^{+0.0353}_{-0.0235}$

(*Continued.*)

Experiment	h_L/H	h_U/H	ρ_C	ρ_L	ρ_U	ρ_0	E_{p0}
H1	0.231	0.769	1.0400	1.0925	1.0243	$0.9955^{+0.0002}_{-0.0002}$	$6.3578^{+0.0353}_{-0.0432}$
H2	0.286	0.714	1.0400	1.0738	1.0265	$0.9958^{+0.0001}_{-0.0001}$	$6.7840^{+0.0157}_{-0.0235}$
H3	0.375	0.625	1.0400	1.0550	1.0310	$0.9960^{+0.0002}_{-0.0002}$	$7.5213^{+0.0471}_{-0.0314}$
H4	0.444	0.556	1.0400	1.4560	1.0355	$0.9963^{+0.0003}_{-0.0002}$	$8.0795^{+0.0432}_{-0.0549}$
I1	0.114	0.886	1.0400	1.1135	1.0306	$0.9964^{+0.0002}_{-0.0002}$	$6.9115^{+0.0392}_{-0.0392}$
I2	0.146	0.854	1.0400	1.0873	1.0319	$0.9962^{+0.0003}_{-0.0002}$	$7.2330^{+0.0432}_{-0.0549}$
I3	0.205	0.795	1.0400	1.0610	1.0346	$0.9966^{+0.0002}_{-0.0002}$	$7.6645^{+0.0471}_{-0.0314}$
I4	0.255	0.745	1.0400	1.0479	1.0373	$0.9966^{+0.0001}_{-0.0003}$	$8.1245^{+0.0549}_{-0.0235}$
J1	0.310	0.690	1.0400	1.0820	1.0211	$0.9966^{+0.0001}_{-0.0002}$	$5.9656^{+0.0314}_{-0.0275}$
K1	0.660	0.340	1.0400	1.0563	1.0082	$0.9948^{+0.0000}_{-0.0001}$	$6.7522^{+0.0196}_{-0.0000}$
K2	0.464	0.536	1.0400	1.0727	1.0118	$0.9952^{+0.0001}_{-0.0001}$	$5.8190^{+0.0196}_{-0.0196}$
K3	0.335	0.665	1.0400	1.0890	1.0153	$0.9951^{+0.0000}_{-0.0000}$	$5.5877^{+0.0000}_{-0.0000}$
K4	0.245	0.755	1.0400	1.1053	1.0188	$0.9951^{+0.0000}_{-0.0000}$	$5.6726^{+0.0000}_{-0.0000}$
K5	0.178	0.822	1.0400	1.1217	1.0224	$0.9949^{+0.0000}_{-0.0001}$	$6.0024^{+0.0196}_{-0.0000}$
K6	0.126	0.874	1.0400	1.1380	1.0259	$0.9950^{+0.0000}_{-0.0000}$	$6.4087^{+0.0000}_{-0.0000}$
K7	0.085	0.915	1.0400	1.1543	1.0294	$0.9950^{+0.0001}_{-0.0001}$	$6.9284^{+0.0196}_{-0.0196}$

experimental setup, at least five repeated runs were performed to make qualitative and quantitative observations. The height and length of the two-layer density-stratified heavy fluid, H and L_0, remained fixed for all experiments.

A. Gravity currents produced from a homogeneous source, $R_\rho = 1$

We begin with the case in which the gravity current was produced from a homogeneous buoyancy source, $R_\rho = 1$. The densities of heavy and ambient light fluids were chosen at $\rho_C = 1.0400$ g cm^{-3} and $\rho_0 = 0.9967$ g cm^{-3}, respectively, and Re $\approx 53\,000$.

1. Qualitative and quantitative results

The heavy fluid was set into motion when the gate was withdrawn. Since the lock length L_0 is short compared with the lock height H, the gravity current moves quickly from the initial condition into the inertial phase. The images for the gravity current produced from a homogeneous source in experiment $02/02/15 - A1$ with $g'_0 = 42.62$ cm s^{-2} are presented in Fig. 2. With the images as presented in Fig. 2, the front location can be identified without ambiguity as the furthest point reached by the gravity current. The front velocity can then be calculated as the time rate of change of the front location. Figure 3(a) shows the front velocity history of the gravity current produced from a homogeneous source in experiment $02/02/15 - A1$.

In this experiment, the gravity current produced from a homogeneous buoyancy source reaches its maximum front velocity $U_{f\,\text{max}} \approx 13.62$ cm s^{-1} at $t \approx 2.0$ s. When reaching the maximum front velocity, the front has accelerated for approximately 2.6 lock lengths. During $2.0 \lesssim t \lesssim 6.0$ s, the front velocity decreases slightly from the maximum front velocity and the gravity current is known to be in the slumping phase, since the disturbance reflected from the left wall has not caught up with the front. At $t \approx 6.0$ s, the arrival of the reflected disturbance at the front initiates the transition to the inertial phase, as reported by Ref. [54]. When the transition to the inertial phase occurs, the front has traveled approximately 7.8 lock lengths. The irregularity of the contour on the top of the head in the inertial phase, as shown in Fig. 2, is due to shear instabilities [3].

TABLE II. Table showing experimental constants, including the density difference ratio, R_ρ, buoyancy distribution parameter, R_B, Froude number in the inertial phase, F_I, t-intercept in the 3/2 power relationship (7), t_I, front location at which the maximum front velocity is reached, $x_{f\,\text{max}}$, and maximum front velocity, $U_{f\,\text{max}}$. Each experimental setup is repeated at least five times. The error estimates are to add and subtract the maximum and minimum values and are not the r.m.s. estimates.

Experiment	R_ρ	R_B	F_I	$-t_I$ (s)	$x_{f\,\text{max}}$ (cm)	$U_{f\,\text{max}}$ (cm s^{-1})
A1	1.000	–	$1.33^{+0.02}_{-0.02}$	$1.60^{+0.12}_{-0.17}$	$20.93^{+5.32}_{-1.82}$	$13.52^{+0.26}_{-0.25}$
B1	0.872	0.777	$1.35^{+0.04}_{-0.05}$	$1.71^{+0.17}_{-0.07}$	$26.04^{+1.23}_{-0.82}$	$13.55^{+0.34}_{-0.26}$
B2	0.768	0.754	$1.32^{+0.01}_{-0.02}$	$1.61^{+0.14}_{-0.15}$	$27.14^{+4.98}_{-1.95}$	$13.69^{+0.09}_{-0.28}$
B3	0.681	0.732	$1.31^{+0.02}_{-0.02}$	$1.56^{+0.41}_{-0.24}$	$24.68^{+4.22}_{-4.62}$	$13.87^{+0.28}_{-0.37}$
B4	0.608	0.709	$1.31^{+0.03}_{-0.03}$	$1.53^{+0.06}_{-0.10}$	$22.48^{+3.58}_{-2.46}$	$14.05^{+0.33}_{-0.36}$
B5	0.546	0.686	$1.28^{+0.02}_{-0.03}$	$1.28^{+0.19}_{-0.20}$	$22.47^{+4.89}_{-2.08}$	$14.38^{+0.44}_{-0.30}$
B6	0.492	0.663	$1.29^{+0.02}_{-0.04}$	$1.39^{+0.20}_{-0.16}$	$23.37^{+8.36}_{-2.56}$	$14.46^{+0.30}_{-0.34}$
B7	0.445	0.640	$1.25^{+0.02}_{-0.03}$	$1.15^{+0.29}_{-0.12}$	$23.34^{+3.45}_{-2.07}$	$14.58^{+0.45}_{-0.42}$
B8	0.403	0.617	$1.25^{+0.03}_{-0.03}$	$1.28^{+0.22}_{-0.22}$	$23.83^{+4.07}_{-2.95}$	$14.47^{+0.26}_{-0.31}$
B9	0.253	0.503	$1.17^{+0.02}_{-0.01}$	$0.80^{+0.14}_{-0.13}$	$22.93^{+0.93}_{-1.38}$	$15.32^{+0.31}_{-0.27}$
C1	0.829	0.554	$1.32^{+0.03}_{-0.05}$	$1.43^{+0.14}_{-0.18}$	$22.02^{+4.50}_{-1.66}$	$14.40^{+0.25}_{-0.30}$
C2	0.690	0.509	$1.30^{+0.02}_{-0.02}$	$1.28^{+0.07}_{-0.07}$	$21.11^{+0.93}_{-0.60}$	$14.54^{+0.13}_{-0.16}$
C3	0.575	0.463	$1.27^{+0.02}_{-0.01}$	$1.17^{+0.04}_{-0.10}$	$24.93^{+3.58}_{-4.25}$	$14.50^{+0.14}_{-0.16}$
C4	0.478	0.417	$1.24^{+0.03}_{-0.03}$	$1.04^{+0.07}_{-0.17}$	$23.90^{+4.22}_{-2.75}$	$14.89^{+0.31}_{-0.35}$
C5	0.394	0.372	$1.22^{+0.02}_{-0.03}$	$0.80^{+0.17}_{-0.11}$	$25.02^{+4.13}_{-2.97}$	$15.03^{+0.22}_{-0.17}$
C6	0.322	0.326	$1.21^{+0.05}_{-0.05}$	$0.65^{+0.35}_{-0.26}$	$26.39^{+7.34}_{-3.75}$	$15.26^{+0.26}_{-0.28}$
C7	0.260	0.280	$1.17^{+0.02}_{-0.03}$	$0.34^{+0.08}_{-0.12}$	$28.04^{+1.93}_{-6.11}$	$15.22^{+0.24}_{-0.27}$
C8	0.204	0.235	$1.14^{+0.03}_{-0.04}$	$0.07^{+0.18}_{-0.18}$	$23.11^{+1.51}_{-1.02}$	$15.69^{+0.20}_{-0.23}$
D1	0.744	0.332	$1.30^{+0.01}_{-0.01}$	$1.25^{+0.12}_{-0.06}$	$22.85^{+3.93}_{-1.53}$	$14.47^{+0.23}_{-0.30}$
D2	0.535	0.263	$1.26^{+0.01}_{-0.01}$	$0.96^{+0.10}_{-0.07}$	$22.93^{+5.53}_{-2.11}$	$14.76^{+0.15}_{-0.12}$
D3	0.362	0.195	$1.24^{+0.02}_{-0.02}$	$0.67^{+0.11}_{-0.07}$	$22.55^{+0.61}_{-0.45}$	$15.26^{+0.16}_{-0.15}$
D4	0.216	0.126	$1.24^{+0.04}_{-0.05}$	$0.44^{+0.07}_{-0.12}$	$22.65^{+0.63}_{-1.08}$	$15.38^{+0.23}_{-0.29}$
D5	0.891	0.373	$1.33^{+0.05}_{-0.04}$	$1.48^{+0.13}_{-0.10}$	$21.51^{+4.68}_{-1.54}$	$14.12^{+0.29}_{-0.24}$
E1	0.488	0.109	$1.29^{+0.02}_{-0.01}$	$1.06^{+0.09}_{-0.12}$	$22.96^{+5.08}_{-2.47}$	$14.48^{+0.29}_{-0.42}$
E2	0.782	0.163	$1.32^{+0.02}_{-0.02}$	$1.33^{+0.08}_{-0.09}$	$21.52^{+0.80}_{-1.12}$	$14.50^{+0.09}_{-0.19}$
E3	0.888	0.182	$1.34^{+0.04}_{-0.03}$	$1.45^{+0.24}_{-0.15}$	$21.20^{+0.68}_{-0.70}$	$14.29^{+0.18}_{-0.20}$
E4	0.398	0.090	$1.28^{+0.01}_{-0.01}$	$1.00^{+0.03}_{-0.03}$	$21.86^{+0.30}_{-0.48}$	$14.70^{+0.16}_{-0.14}$
F1	0.300	0.100	$1.25^{+0.02}_{-0.02}$	$0.65^{+0.11}_{-0.11}$	$22.23^{+0.55}_{-0.22}$	$14.93^{+0.07}_{-0.17}$
F2	0.400	0.100	$1.29^{+0.02}_{-0.02}$	$1.00^{+0.21}_{-0.12}$	$23.04^{+4.47}_{-1.96}$	$14.68^{+0.28}_{-0.37}$
F3	0.600	0.100	$1.31^{+0.03}_{-0.02}$	$1.23^{+0.13}_{-0.14}$	$21.53^{+0.84}_{-0.95}$	$14.38^{+0.17}_{-0.13}$
F4	0.800	0.100	$1.34^{+0.02}_{-0.03}$	$1.40^{+0.10}_{-0.10}$	$21.84^{+0.84}_{-0.48}$	$14.34^{+0.04}_{-0.09}$
G1	0.300	0.300	$1.15^{+0.03}_{-0.02}$	$0.14^{+0.08}_{-0.13}$	$24.06^{+0.99}_{-0.45}$	$15.64^{+0.17}_{-0.19}$
G2	0.400	0.300	$1.21^{+0.03}_{-0.03}$	$0.53^{+0.12}_{-0.12}$	$22.90^{+0.50}_{-0.38}$	$15.17^{+0.08}_{-0.12}$
G3	0.600	0.300	$1.26^{+0.01}_{-0.03}$	$1.02^{+0.12}_{-0.09}$	$22.48^{+0.41}_{-1.12}$	$14.55^{+0.26}_{-0.21}$
G4	0.800	0.300	$1.34^{+0.03}_{-0.02}$	$1.34^{+0.16}_{-0.16}$	$21.91^{+1.11}_{-1.15}$	$14.34^{+0.23}_{-0.37}$
H1	0.300	0.500	$1.17^{+0.02}_{-0.02}$	$0.69^{+0.17}_{-0.11}$	$23.48^{+1.38}_{-0.90}$	$15.31^{+0.10}_{-0.11}$
H2	0.400	0.500	$1.21^{+0.01}_{-0.02}$	$0.81^{+0.12}_{-0.08}$	$22.77^{+0.78}_{-0.92}$	$14.96^{+0.32}_{-0.46}$
H3	0.600	0.500	$1.26^{+0.02}_{-0.02}$	$1.06^{+0.12}_{-0.10}$	$21.55^{+1.44}_{-0.81}$	$14.55^{+0.33}_{-0.20}$

(*Continued.*)

Experiment	R_ρ	R_B	F_I	$-t_I$ (s)	$x_{f\,max}$ (cm)	$U_{f\,max}$ (cm s^{-1})
H4	0.800	0.500	$1.32^{+0.05}_{-0.03}$	$1.38^{+0.27}_{-0.12}$	$21.12^{+0.80}_{-0.64}$	$14.19^{+0.15}_{-0.22}$
I1	0.300	0.700	$1.25^{+0.04}_{-0.02}$	$1.34^{+0.16}_{-0.08}$	$22.04^{+1.05}_{-0.68}$	$14.38^{+0.22}_{-0.30}$
I2	0.400	0.700	$1.27^{+0.04}_{-0.03}$	$1.33^{+0.12}_{-0.10}$	$21.46^{+0.78}_{-0.41}$	$14.45^{+0.11}_{-0.19}$
I3	0.600	0.700	$1.30^{+0.02}_{-0.02}$	$1.35^{+0.18}_{-0.11}$	$20.63^{+1.68}_{-1.24}$	$14.22^{+0.44}_{-0.49}$
I4	0.800	0.700	$1.33^{+0.01}_{-0.02}$	$1.57^{+0.11}_{-0.10}$	$20.00^{+0.56}_{-0.61}$	$13.82^{+0.14}_{-0.17}$
J1	0.300	0.400	$1.16^{+0.02}_{-0.02}$	$0.54^{+0.14}_{-0.11}$	$22.05^{+0.60}_{-0.62}$	$15.05^{+0.12}_{-0.13}$
K1	0.216	0.100	$1.22^{+0.02}_{-0.03}$	$0.07^{+0.15}_{-0.35}$	$23.42^{+6.01}_{-2.20}$	$15.16^{+0.35}_{-0.24}$
K2	0.216	0.200	$1.17^{+0.02}_{-0.03}$	$0.04^{+0.04}_{-0.03}$	$23.82^{+0.93}_{-0.43}$	$15.69^{+0.38}_{-0.32}$
K3	0.216	0.300	$1.14^{+0.02}_{-0.03}$	$0.08^{+0.10}_{-0.04}$	$25.18^{+5.17}_{-2.41}$	$15.86^{+0.43}_{-0.39}$
K4	0.216	0.400	$1.12^{+0.02}_{-0.04}$	$0.28^{+0.40}_{-0.24}$	$25.43^{+4.19}_{-1.85}$	$15.65^{+0.24}_{-0.17}$
K5	0.216	0.500	$1.14^{+0.02}_{-0.03}$	$0.61^{+0.22}_{-0.22}$	$23.87^{+1.34}_{-0.97}$	$15.76^{+0.36}_{-0.39}$
K6	0.216	0.600	$1.18^{+0.04}_{-0.04}$	$0.93^{+0.18}_{-0.21}$	$24.75^{+0.47}_{-0.37}$	$15.43^{+0.43}_{-0.46}$
K7	0.216	0.700	$1.22^{+0.03}_{-0.05}$	$1.20^{+0.22}_{-0.12}$	$22.96^{+1.84}_{-2.32}$	$14.44^{+0.17}_{-0.32}$

Figure 3(b) shows the relationship between $x_f^{3/2}$ and t for experiment $02/02/15 - A1$. During $0 \leqslant t \lesssim 6.0$ s, namely, during the initial acceleration and the slumping phase, the approach of front location data to the $3/2$ power relationship (7) is from above. The presence of the inertial phase is
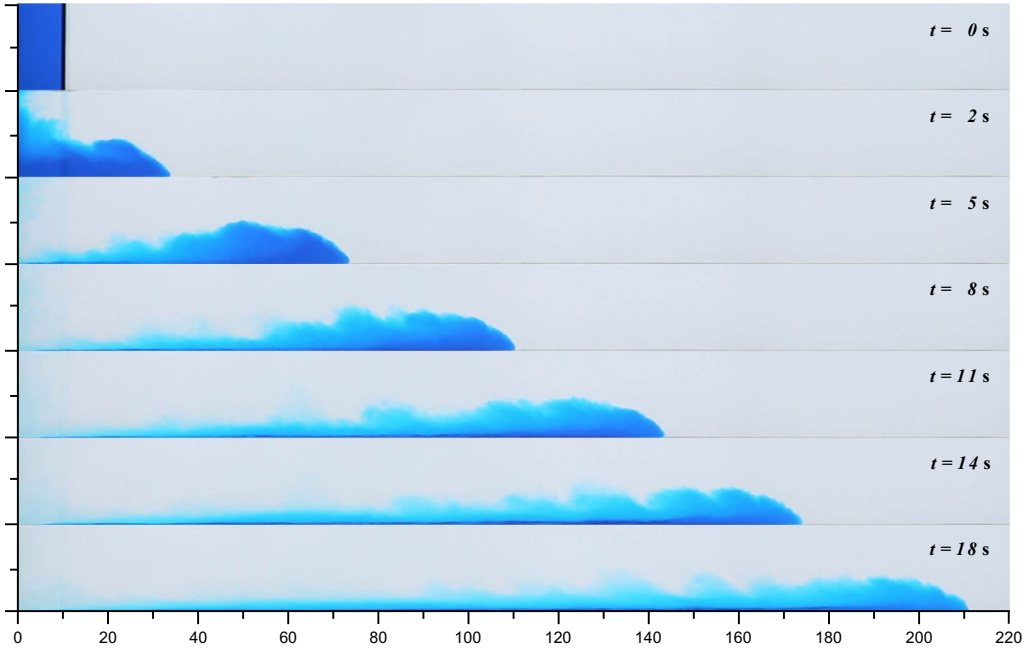
FIG. 2. Experiment $02/02/15 - A1$: flow images for the gravity current produced from a homogeneous buoyancy source with $H = 20$ cm, $L_0 = 10$ cm, and $g'_0 = 42.62$ cm s^{-2} propagating on a horizontal boundary. Distances in x and y directions are in units of cm. Time instances in the images are chosen at $t = 0, 2, 5, 8, 11, 14, 18$ s. In this experiment the maximum front velocity $U_{f\,max} \approx 13.62$ cm s^{-1} occurs at $t \approx 2.0$ s, and the inertial phase begins at $t \approx 6.0$ s.
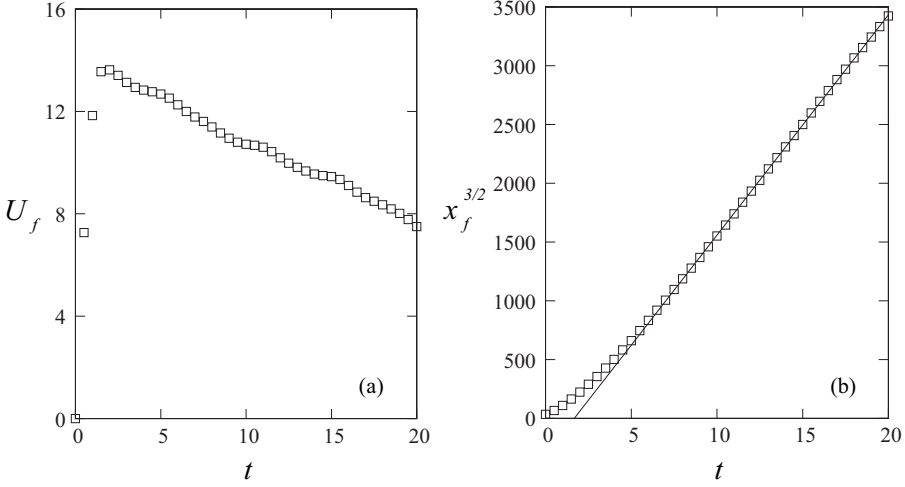
FIG. 3. Experiment $02/02/15 - A1$: front velocity history, shown in panel (a), and relationship between $x_f^{3/2}$ and t, shown in panel (b), for the gravity current produced from a homogeneous buoyancy source. The front velocity is in units of cm s^{-1}, the front location is in units of cm and time is in s. The solid line in (b) represents the straight line of best fit to the inertial phase of propagation, and the fitting equation is $x_f^{3/2} = 187.35(t + t_I)$, where $t_I = -1.68$ s. See the caption of Fig. 2 for other details.

best described by the straight line in Fig. 3(b), where the $3/2$ power relationship (7) applies. The slope of the fitting line represents $1.5 F_I B_0^{1/2}$ and the Froude number in the inertial phase, F_I, can be calculated based on the slope of the fitting line and the total buoyancy B_0 in the experiment. Table II lists the values of F_I in this and other experiments.

It is clear that the front location data robustly follow the $3/2$ power relationship (7) in the inertial phase, where $F_I = 1.33 \pm 0.02$ is observed for the gravity currents produced from a homogeneous buoyancy source. The running length of the channel is not sufficiently long so that the gravity currents produced from a homogeneous buoyancy source have not reached the viscous phase in this experiment.

B. Gravity currents produced from a weakly stratified source, $0.4 \lesssim R_\rho < 1$

We now turn the attention to the situation when the stratification is weak, i.e., that the density difference between the two layers is relatively small so that the mixing between the layers is more immediate in the inertial phase, and make careful observations of the flow morphology in two cases. The first case is when the lower layer contains more buoyancy than the upper layer, i.e., $0 < R_B < 0.5$, and the second case is when the upper layer contains more buoyancy than the lower layer, $0.5 < R_B < 1$. In the experiments, the occurrence of the inertial phase is defined as the time when the front location data match the $3/2$ power relationship and is indicated in the figure caption of the flow images for reference.

1. Qualitative features

Visualization with the help of dyed layers, where the lower and upper layers are dyed blue and yellow, respectively, allows observation of the slumping and the following propagation of gravity currents. The choice of using blue and yellow colors makes it easy to identify the region where the fluids from the two layers mix, as indicated by the green color. After the gate is removed from the lock, the heavy fluid collapses out of the lock region sequentially, with the lower layer leaving first to form the front and the upper layer leaving lastly to form the body and tail of the currents.
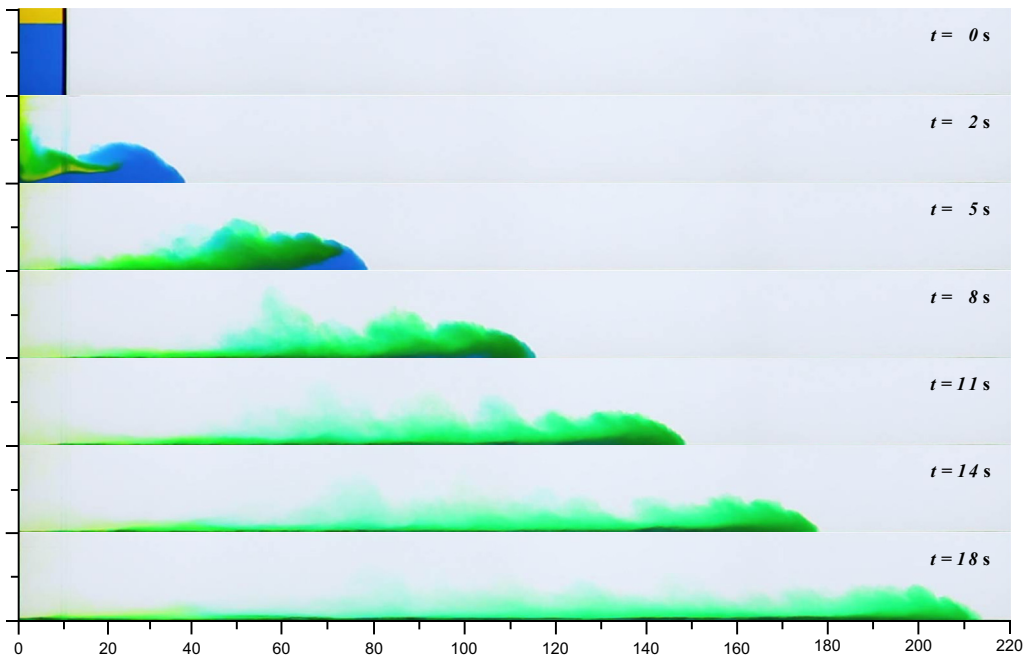
FIG. 4. Experiment $08/20/15 - E3$: flow images for the gravity current produced from a weakly stratified buoyancy source with $R_\rho = 0.888$ and $R_B = 0.182$ propagating on a horizontal boundary. Distances in x and y directions are in units of cm. Time instances in the images are chosen at $t = 0, 2, 5, 8, 11, 14, 18$ s. In this experiment the maximum front velocity $U_{f\,\mathrm{max}} \approx 14.25$ cm s^{-1} occurs at $t \approx 1.5$ s, and the inertial phase begins at $t \approx 5.5$ s.

For gravity currents produced from a weakly stratified source, Fig. 4 shows the images for experiment $08/20/15 - E3$ with $R_\rho = 0.888$ and $R_B = 0.182$ and Fig. 5 shows the images for experiment $03/19/15 - B1$ with $R_\rho = 0.872$ and $R_B = 0.777$. There exist slight differences in the flow evolution towards the inertial phase between the two cases upon further scrutiny.

When the upper layer contains less buoyancy than the lower layer, $0 < R_B < 0.5$, the upper layer forms a wedge-shaped intrusion, which extends into the head between the body and wake region of the gravity current, as shown in Fig. 4 for experiment $08/20/15 - E3$ with $R_\rho = 0.888$ and $R_B = 0.182$. By the time $t \approx 8$ s in the inertial phase, the fluids from the two layers in the gravity current head already mix thoroughly, as shown by the green color in the images in Fig. 4. On the other hand, when the lower layer contains less buoyancy than the upper layer, $0.5 < R_B < 1$, the upper layer likewise intrudes between the body and wake region but quickly overrides and outruns the lower layer. Since the density contrast is relatively small, the fluids from the two layers mix as the upper layer overrides the lower layer during the propagation, as shown by the green color in the images in Fig. 5 for experiment $03/19/15 - B1$ with $R_\rho = 0.872$ and $R_B = 0.777$. There does not appear to be a clear transition between the preceding two cases as the buoyancy distribution parameter varies from $R_B \to 0$ to $R_B \to 1$, and the gravity current head ultimately becomes homogeneous towards the inertial phase for gravity currents produced from a weakly stratified buoyancy source.

2. Quantitative results

For gravity currents produced from a weakly stratified source, the fluids from the two layers in the head region mix thoroughly in the inertial phase, irrespective of the initial distribution of buoyancy between the layers. Since the front velocity history and the relationship between $x_f^{3/2}$ and t are both observed to be qualitatively similar for all experiments when the two-layer buoyancy source is
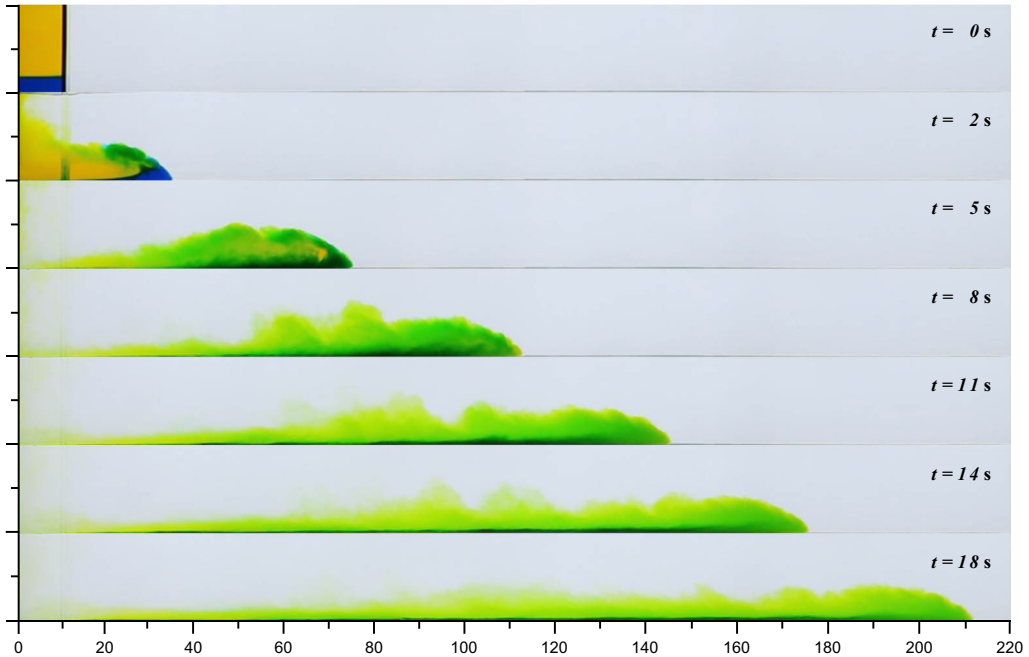
FIG. 5. Experiment $03/19/15 - B1$: flow images for the gravity current produced from a weakly stratified buoyancy source with $R_\rho = 0.872$ and $R_B = 0.777$ propagating on a horizontal boundary. Distances in x and y directions are in units of cm. Time instances in the images are chosen at $t = 0,2,5,8,11,14,18$ s. In this experiment the maximum front velocity $U_{f\,max} \approx 13.53$ cm s^{-1} occurs at $t \approx 2.0$ s, and the inertial phase begins at $t \approx 6.0$ s.

weakly stratified, only the quantitative results from experiment $08/20/15 - E3$ with $R_\rho = 0.888$ and $R_B = 0.182$ are presented in detail for illustrative purposes while results from other weakly stratified buoyancy sources are omitted for brevity. The operational parameters and experimental constants for other gravity currents produced from a weakly stratified source are also listed in Table I and Table II.

Figure 6 shows the front velocity history and the relationship between $x_f^{3/2}$ and t for experiment $08/20/15 - E3$ with $R_\rho = 0.888$ and $R_B = 0.182$. After the heavy fluid is released, the produced gravity current accelerates and quickly moves into the inertial phase, as described previously for gravity currents produced from a homogeneous source. When reaching the maximum front velocity $U_{f\,max} \approx 14.25$ cm s^{-1} at $t \approx 1.5$ s, the front has accelerated for approximately 2.1 lock lengths. It is worth noting that in Fig. 6(b) the approach of front location data to the 3/2 power relationship, in the plot of $x_f^{3/2}$ against t, is gradual from above and is similar to the approach observed previously for gravity currents produced from a homogeneous source. The Froude number in the inertial phase, F_I, can be derived from the slope of the best fit line to the inertial phase, and it is found that $F_I = 1.31$ in this experiment. As will be discussed later, the Froude number in the inertial phase depends on both the density difference ratio, R_ρ, and the buoyancy distribution parameter, R_B. However, for gravity currents produced from a weakly stratified source, the dependence of the Froude number on R_ρ and R_B is less obvious compared with that for gravity currents produced from a strongly stratified source. In fact, the Froude number in the inertial phase assumes its maximum value at $F_I = 1.33 \pm 0.02$ for gravity currents produced from a homogeneous source, $R_\rho = 1$.

C. Gravity currents produced from a strongly stratified source, $0 < R_\rho \lesssim 0.4$

In this section, we focus on the gravity currents produced from a strongly stratified source, i.e., the density contrast between the two layers is larger so that there is less mixing between the
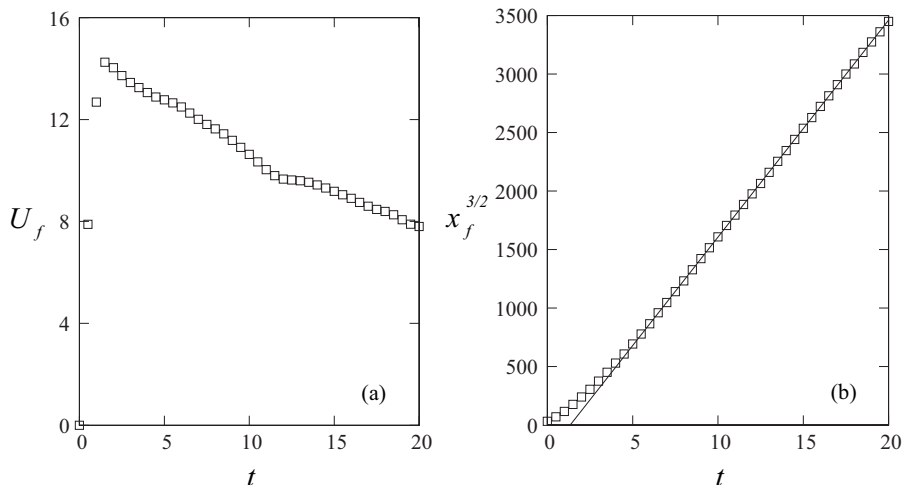
FIG. 6. Experiment $08/20/15 - E3$: front velocity history, panel (a), and relationship between $x_f^{3/2}$ and t, panel (b), for gravity current produced from a weakly stratified buoyancy source with $R_\rho = 0.888$ and $R_B = 0.182$ propagating on a horizontal boundary. The front velocity is in units of cm s^{-1}, the front location is in units of cm and time is in s. The solid line in (b) represents the straight line of best fit to the inertial phase of propagation and the fitting equation is $x_f^{3/2} = 185.42(t + t_I)$, where $t_I = -1.34$ s. See the caption of Fig. 4 for other details.

layers compared with that observed in the gravity currents produced from a weakly stratified source. Three different cases, which encompass different flow morphologies observed for gravity currents produced from a strongly stratified source, are presented in order. The first case is when the flow is dominated by the lower layer, $R_B \to 0$, the second case is when the flow is dominated by the upper layer, $R_B \to 1$, and the third case is a special transition between the two preceding cases, in which the flow is neither dominated by the lower layer nor dominated by the upper layer and the buoyancy distribution parameter falls in the range of $0.3 \lesssim R_B \lesssim 0.5$. As argued theoretically in Sec. II, the time scale of separation is shorter than that of mixing when the stratification is strong for flows dominated by the upper layer and for flows dominated by the lower layer. However, an exceptional case exists such that the time scale of separation can be greater than that of mixing provided $B_L \approx B_U$ even when the stratification between the layers is strong.

1. Qualitative results

As reported for gravity currents produced from a weakly stratified source, the gravity currents produced from a strongly stratified source slump in a similar fashion. The lower layer and the upper layer leave the lock region sequentially to form the front and body of the flow, respectively.

For gravity currents produced from a strongly stratified source, Fig. 7 shows the images for experiment $08/06/15 - D4$ with $R_\rho = 0.216$ and $R_B = 0.126$ and Fig. 8 shows the images for experiment $10/21/16 - K6$ with $R_\rho = 0.216$ and $R_B = 0.600$. However, the flow evolutions are intrinsically different between the case when the flow is dominated by the lower layer, $R_B \to 0$, and the case when the flow is dominated by the upper layer, $R_B \to 1$.

For gravity currents produced from a strongly stratified source and when the flow is dominated by the lower layer, $R_B \to 0$, the upper layer leaves the lock region last in the slumping process and remains in the tail region of the currents throughout the propagation, as shown in Fig. 7 for experiment $08/06/15 - D4$ with $R_\rho = 0.216$ and $R_B = 0.126$. Mixing between the layers, which occurs only on top of the tail currents, is very limited. As clearly shown in Fig. 7, the two layers separate into two regions with streamwise stratification. On the other hand, when the flow is dominated by the
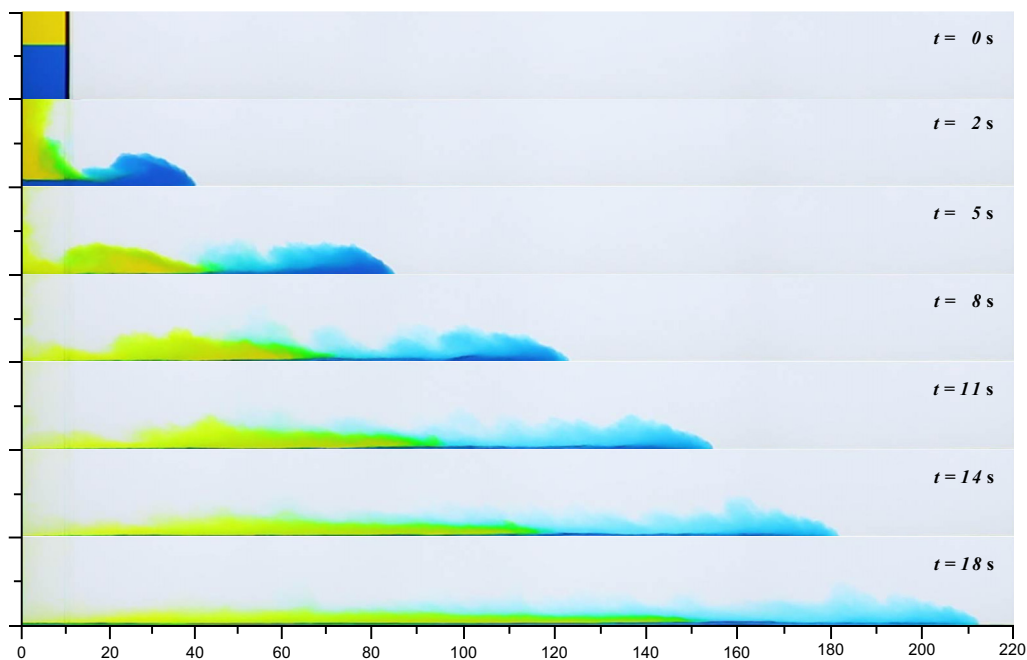
FIG. 7. Experiment $08/06/15 - D4$: flow images for the gravity current produced from a strongly stratified buoyancy source with $R_\rho = 0.216$ and $R_B = 0.126$ propagating on a horizontal boundary. Distances in x and y directions are in units of cm. Time instances in the images are chosen at $t = 0, 2, 5, 8, 11, 14, 18$ s. In this experiment the maximum front velocity $U_{f \max} \approx 15.23$ cm s^{-1} occurs at $t \approx 1.5$ s, and the inertial phase begins at $t \approx 7.0$ s.

upper layer, $R_B \to 1$, initially in the slumping process the lower layer takes the lead. The upper layer leaves the lock region lastly but overrides and outruns the leading lower layer during the propagation, as shown in Fig. 8 for experiment $10/21/16 - K6$ with $R_\rho = 0.216$ and $R_B = 0.600$. It is interesting to note that when the upper layer overrides and outruns the lower layer, the size of the gravity current head increases rapidly and a larger scale Kelvin-Helmholtz instability occurs along the interface between the moving heavy fluid and ambient light fluid. Also, a special form of mixing develops during the propagation. As shown in Fig. 8 at $t = 2$ s and somewhat faintly at $t = 5$ s, the upper layer, which is represented by the yellow color, is overrunning the lower layer and overlain by a region of green color, which demonstrates that the mixture of fluids from the two layers has been lifted up to the upper edge of the gravity current head.

For gravity currents produced from a strongly stratified source of which the buoyancy distribution parameter falls in the range of $0.3 \lesssim R_B \lesssim 0.5$, Fig. 9 shows the images for experiment $09/30/16 - K4$ with $R_\rho = 0.216$ and $R_B = 0.400$. It is evident that while part of the fluid in the upper layer remains unmixed in the tail region, the fluids from the two layers move forward in the head without separation for an extended period and mixing of the fluids in the head region is enhanced.

2. Quantitative results

Figure 10 shows the front velocity history and Fig. 11 shows the relationship between $x_f^{3/2}$ and t for experiment $08/06/15 - D4$ with $R_\rho = 0.216$ and $R_B = 0.126$. In this experiment, the flow is dominated by the lower layer, and the upper layer is persistently left in the tail region throughout the propagation. It is observed from the front velocity history that the produced gravity current accelerates and moves into the inertial phase, as previously reported for gravity currents produced from a homogeneous source and from a weakly stratified source. When reaching the maximum
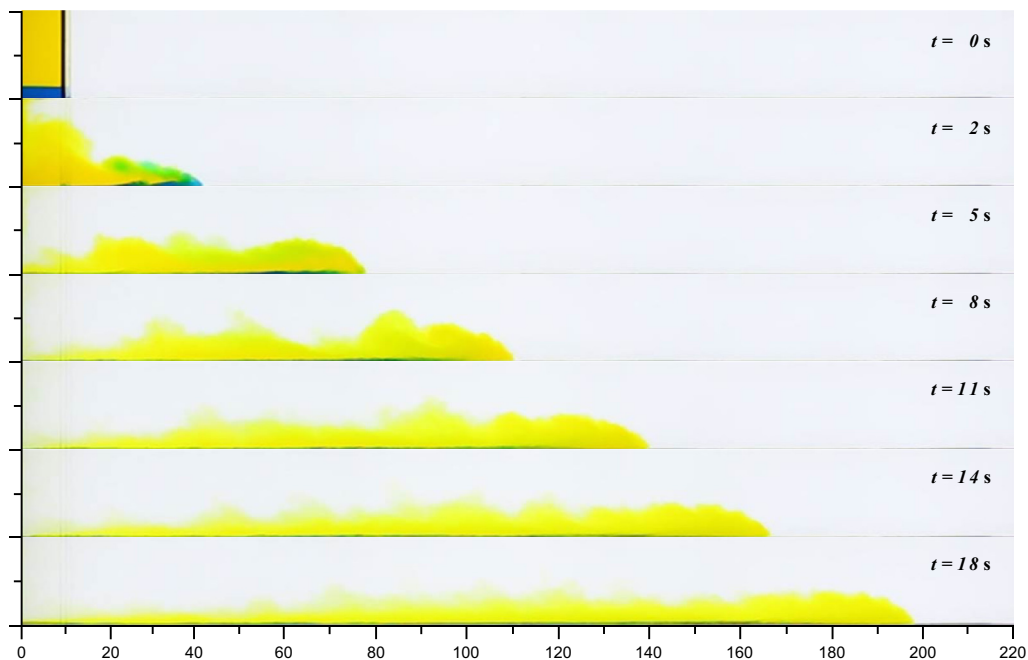
FIG. 8. Experiment $10/21/16 - K6$: flow images for the gravity current produced from a strongly stratified buoyancy source with $R_\rho = 0.216$ and $R_B = 0.600$ propagating on a horizontal boundary. Distances in x and y directions are in units of cm. Time instances in the images are chosen at $t = 0, 2, 5, 8, 11, 14, 18$ s. In this experiment the maximum front velocity $U_{f\,\mathrm{max}} \approx 15.23$ cm s^{-1} occurs at $t \approx 1.5$ s, and the inertial phase begins at $t \approx 6.0$ s.

front velocity $U_{f\,\mathrm{max}} \approx 15.23$ cm s^{-1} at $t \approx 1.5$ s, the front has accelerated for approximately 2.3 lock lengths. The Froude number in the inertial phase, F_I, can be derived from the slope of the best fit line to the inertial phase and it is found that $F_I = 1.28$ in this experiment. However, it is worth noting that, in the plot of $x_f^{3/2}$ against t in Fig. 11, the approach of front location data to the inertial phase is now different. For gravity currents produced from a homogeneous source and from a weakly stratified source, the approach of front location data to the inertial phase is gradual from above in the plot of $x_f^{3/2}$ against t. Here the approach of front location data to the $3/2$ power relationship (7) is from below, as shown in the close-up view in Fig. 11(b). The apparent differences in the approach to the inertial phase suggest that subtle differences in the interaction between the layers exist in the experiments, particularly for gravity currents produced from a strongly stratified source. It should be noted that our results showed good reproducibility. In other words, the observed flow morphologies and approaches to the $3/2$ power relationship are consistent for similar kinds of experiments. Towards the end of the run of experiment $08/06/15 - D4$, deviation of the front location data from the inertial phase represented by (7) in Fig. 11(a) indicates that a transition to the viscous phase has occurred. The Froude number in the inertial phase for gravity currents produced from a strongly stratified source is observed to be persistently lower than that for gravity currents produced from a homogeneous buoyancy source and from a weakly stratified source. Other operational and experimental constants for gravity currents produced from a strongly stratified source are listed in Table I and Table II.

We now present the gravity currents produced from a strongly stratified source and the flow is dominated by the upper layer. Figure 12 shows the front velocity history, and Fig. 13 shows the relationship between $x_f^{3/2}$ and t for experiment $10/21/16 - K6$ with $R_\rho = 0.216$ and $R_B = 0.600$. From the front velocity history, it is observed that the produced gravity current accelerates quickly and
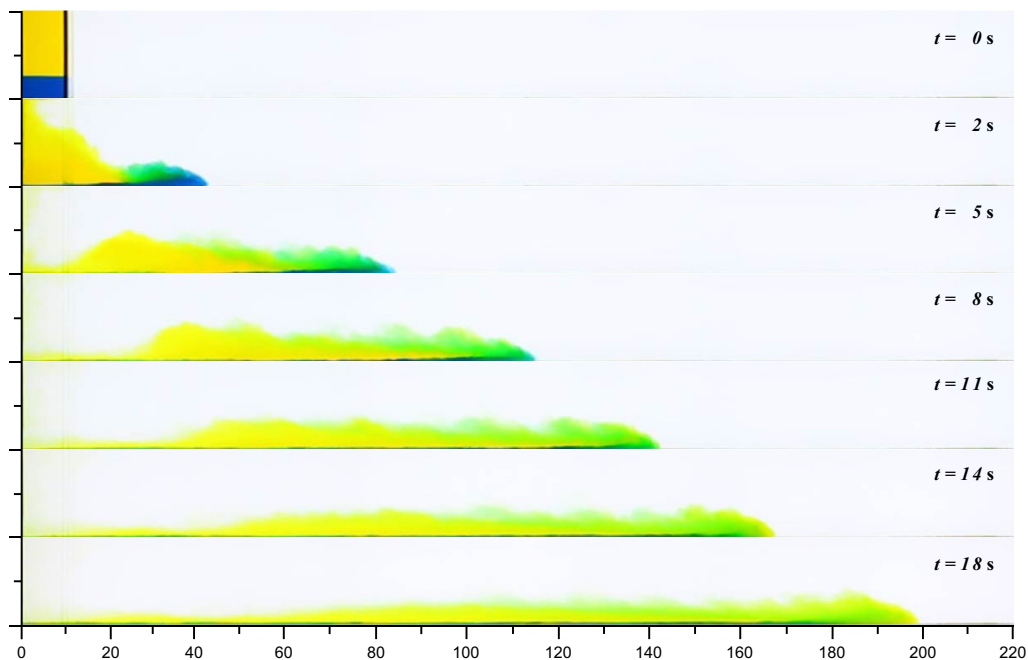
FIG. 9. Experiment $09/30/16 - K4$: flow images for the gravity current produced from a strongly stratified buoyancy source with $R_\rho = 0.216$ and $R_B = 0.400$ propagating on a horizontal boundary. Distances in x and y directions are in units of cm. Time instances in the images are chosen at $t = 0, 2, 5, 8, 11, 14, 18$ s. In this experiment the maximum front velocity $U_{f\,\mathrm{max}} \approx 15.74$ cm s^{-1} occurs at $t \approx 1.5$ s, and the inertial phase begins at $t \approx 2.0$ s.

then decelerates. When reaching the maximum front velocity $U_{f\,\mathrm{max}} \approx 15.23$ cm s^{-1} at $t \approx 1.5$ s, the front has accelerated for approximately 2.5 lock lengths. After reaching the maximum front velocity, the gravity current begins to decelerate. However, front velocity history shows an interesting transient,
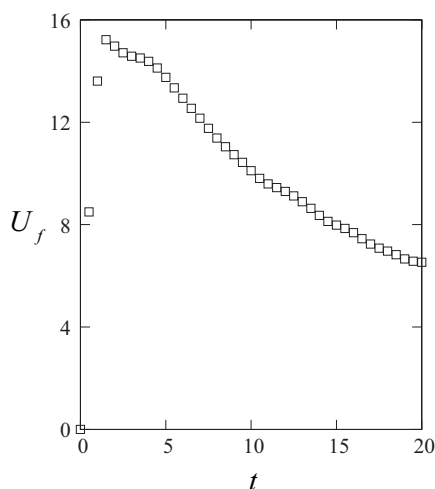
FIG. 10. Experiment $08/06/15 - D4$: front velocity history for the gravity current produced from a strongly stratified buoyancy source with $R_\rho = 0.216$ and $R_B = 0.126$ propagating on a horizontal boundary. The front velocity is in units of cm s^{-1} and time is in s. See the caption of Fig. 7 for other details.
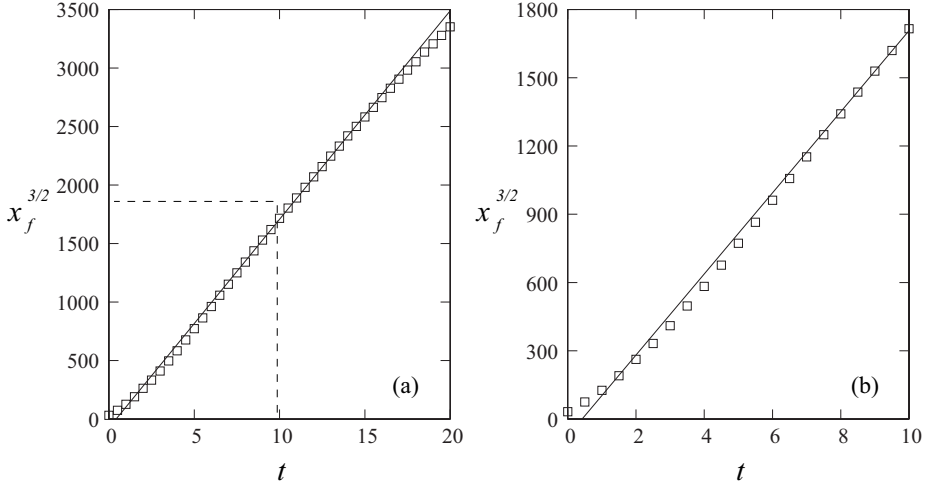
FIG. 11. Experiment $08/06/15 - D4$: relationship between $x_f^{3/2}$ and t for the same experiment shown in Fig. 7. Panel (a) shows the data over the entire time duration of the experiment, and panel (b) shows the close-up view for the beginning and following approach of data to the inertial phase. The front location is in units of cm and time is in s. The solid lines in both panels represent the straight line of best fit to the inertial phase of propagation, and the fitting equation is $x_f^{3/2} = 178.19(t + t_I)$, where $t_I = -0.42$ s. Please also see the captions of Figs. 7 and 10 for other details.

nondecelerating period, $6.0 \lesssim t \lesssim 7.0$ s, during which the upper layer overrides and outruns the lower layer. After this transient, nondecelerating period in the front velocity history, the gravity current continues to move into the inertial phase as represented by the 3/2 power relationship (7) in Fig. 13.

In this experiment $10/21/16 - K6$, the approach of front location data to the 3/2 power relationship (7) in the plot of $x_f^{3/2}$ against t is from above. From the slope of the best fit line in Fig. 13, it is found that $F_I = 1.17$ in this experiment. Towards the end of the run of experiment
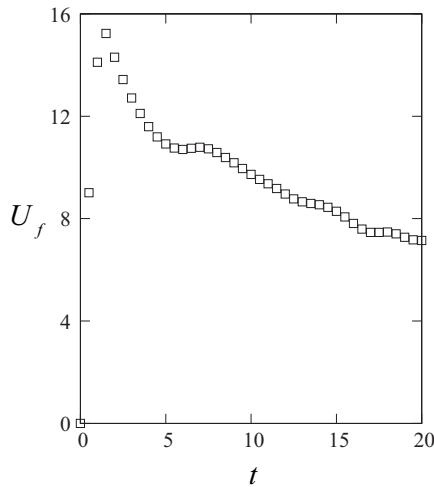
FIG. 12. Experiment $10/21/16 - K6$: front velocity history for the gravity current produced from a strongly stratified buoyancy source with $R_\rho = 0.216$ and $R_B = 0.600$ propagating on a horizontal boundary. The front velocity is in units of cm s^{-1} and time is in s. See the caption of Fig. 8 for other details.
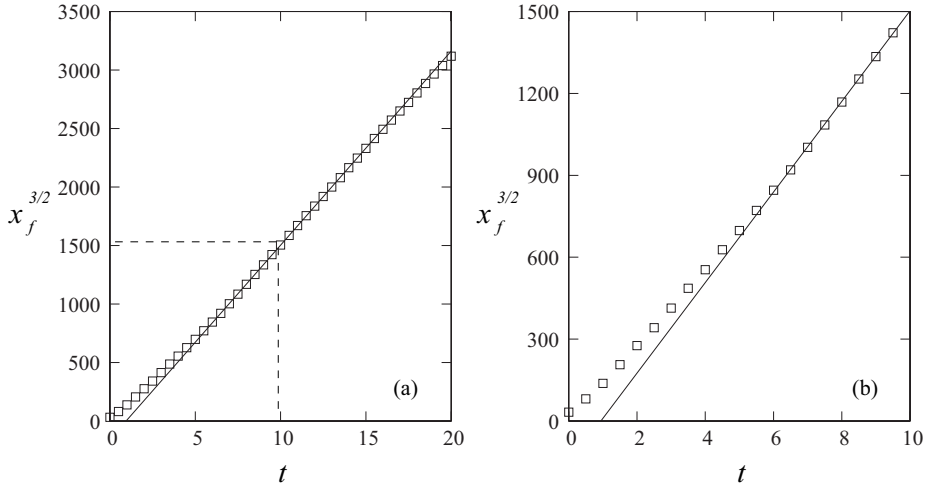
FIG. 13. Experiment $10/21/16 - K6$: relationship between $x_f^{3/2}$ and t for the same experiment shown in Fig. 8. Panel (a) shows the data over the entire time duration of the experiment and panel (b) shows the close-up view for the beginning and following approach of data to the inertial phase. The front location is in units of cm and time is in s. The solid lines in both panels represent the straight line of best fit to the inertial phase of propagation and the fitting equation is $x_f^{3/2} = 165.89(t + t_I)$, where $t_I = -0.94$ s. See the captions of Figs. 8 and 12 for other details.

$10/21/16 - K6$, slight deviation of front location data from the inertial phase again indicates that a transition to the viscous phase has occurred.

Finally, we present the experiment for the gravity currents produced from a strongly stratified source in which the buoyancy distribution parameter falls in the range of $0.3 \lesssim R_B \lesssim 0.5$, such that mixing is enhanced, even though the stratification is strong. Figure 14 shows the front velocity
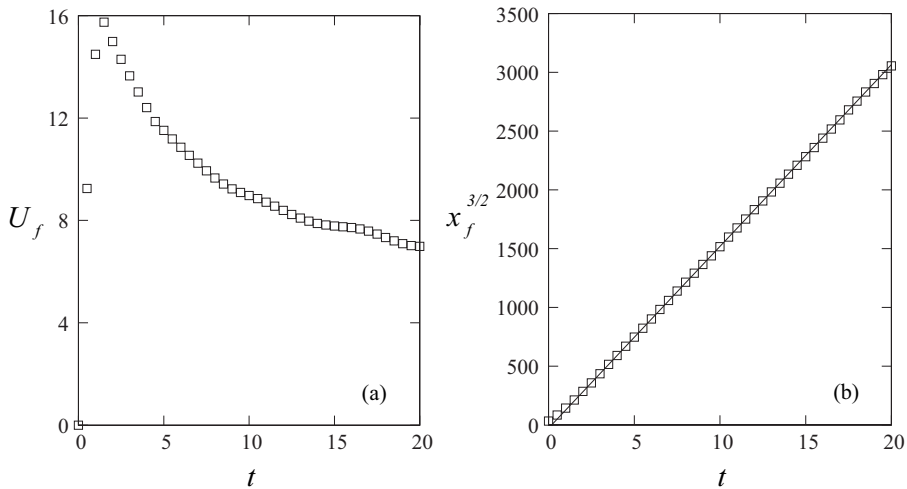
FIG. 14. Experiment $09/30/16 - K4$: front velocity history, panel (a), and relationship between $x_f^{3/2}$ and t, panel (b), for the same experiment shown in Fig. 9. The front velocity is in units of cm s^{-1}, the front location is in units of cm and time is in s. The solid line in (b) represents the straight line of best fit to the inertial phase of propagation and the fitting equation is $x_f^{3/2} = 154.65(t + t_I)$, where $t_I = -0.18$ s. See the caption of Fig. 9 for other details.

history and the relationship between $x_f^{3/2}$ and t for experiment $09/30/16 - K4$ with $R_\rho = 0.216$ and $R_B = 0.400$. This experiment shows a special transition between the flow dominated by the upper layer and the flow dominated by the lower layer. Consistent with the scaling analysis, it is observed that, while part of the upper layer is left in the tail region, the fluids from the two layers move into the head without separation for an extended period and mixing between the fluids in the head region is enhanced.

From the front velocity history, the produced gravity current accelerates and then monotonically decelerates over time in the inertial phase without experiencing a transient, nondecelerating period as in the flow dominated by the upper layer. The 3/2 power relationship (7) also robustly applies in the inertial phase of propagation, as shown in Fig. 14(b), and the approach to the straight line is from above, without going from below as in the flow dominated by the lower layer. In such a special transition case, as observed in Fig. 14(b), the approach of front location data to the 3/2 power relationship (7) is similar to those for gravity currents produced from a homogeneous source and from a weakly stratified source, in which mixing is not suppressed. Furthermore, such an observation confirms the scaling analysis that even when the stratification is strong, mixing can be enhanced provided that $B_L \approx B_U$. Our experiments indicate that such a special transition between $R_B \to 0$ and $R_B \to 1$ occurs when the buoyancy distribution parameter falls in the range of $0.3 \lesssim R_B \lesssim 0.5$. The Froude number in the inertial phase is found to be $F_I = 1.10$, which is calculated from the slope of the straight line in Fig. 14(b).

V. CONCLUSIONS

Experiments on the gravity currents produced from a two-layer density-stratified buoyancy source and a scaling analysis describing the flow morphologies are presented in this paper. The depths of the layers and the densities of fluids in the layers are varied systematically in order to explore the influence of density difference ratio, R_ρ, and buoyancy distribution parameter, R_B, on the Froude number in the inertial phase, F_I, and the flow morphology.

It is observed that, irrespective of the initial conditions of the density difference ratio and the buoyancy distribution parameter, the 3/2 power relationship (7) robustly applies for gravity currents in the inertial phase. For gravity currents produced from a homogeneous source, the approach of front location data to the inertial phase, represented by the 3/2 power relationship (7) in the plot of $x_f^{3/2}$ against t, is gradual from above. For gravity currents produced from a weakly stratified source, the fluids from the two layers mix quickly and thoroughly when the gravity currents move into the inertial phase. For gravity currents produced from a weakly stratified source, the approach of front location data to the 3/2 power relationship (7) in the inertial phase is similar to the case for the gravity currents produced from a homogeneous source. For gravity currents produced from a strongly stratified source, it is observed that, depending on the buoyancy distribution parameter, the flow morphologies in the inertial phase may be qualitatively different. For gravity currents produced from a strongly stratified source, the approach of front location data to the 3/2 power relationship (7) in the inertial phase may be from below when $R_B \to 0$, from above when $0.3 \lesssim R_B \lesssim 0.5$, or gradual from above when $R_B \to 1$. These different approaches to the inertial phase suggest that different interactions between the two layers may exist as the gravity currents propagate.

Indeed, the flow morphology is found to depend on the buoyancy distribution parameter, for gravity currents produced from a weakly stratified source and even more so for gravity currents produced from a strongly stratified source. For gravity currents produced from a strongly stratified source with a dominating lower layer, $R_B \to 0$, the two layers separate and streamwise stratification is created as the gravity currents propagate. For gravity currents produced from a strongly stratified source with a dominating upper layer, $R_B \to 1$, the upper layer may intrude between the forward-propagating lower layer and wake region behind the front, and ultimately outruns the lower layer. For gravity currents produced from a strongly stratified source of which the buoyancy distribution

parameter falls in the range of $0.3 \lesssim R_B \lesssim 0.5$, fluids from the two layers move into the head for an extended period and mixing of fluids in the head region is enhanced.

Our observations on the flow morphology are in concert with the scaling analysis, which essentially describes the mixing and separation processes involved in the gravity currents produced from a two-layer density-stratified buoyancy source. For gravity currents produced from a weakly stratified source, the time scale of mixing is always shorter than that of separation, therefore mixing is more immediate. For gravity currents produced from a strongly stratified source, the time scale of separation is shorter than that of mixing when the flow is dominated by the lower layer, $R_B \rightarrow 0$, and when the flow is dominated by the upper layer, $R_B \rightarrow 1$. However, the time scale of mixing can still be shorter than that of separation even when the buoyancy source is strongly stratified, provided that the buoyancy distribution parameter is in the range of $0.3 \lesssim R_B \lesssim 0.5$. In such an exceptional case, the buoyancy is evenly distributed between the two layers such that the two layers propagate forward at similar speeds, which allows more time for mixing of the fluids from the two layers.

For gravity currents produced from a two-layer density-stratified buoyancy source, it was reported by Ref. [47] that the Froude number in the inertial phase was at $F_I \approx 1.3$ for all two-layer density-stratified buoyancy sources. Our results do not support the Froude number in the inertial phase to be a universal constant. In fact, we found that the Froude number in the inertial phase has its maximum value at $F_I = 1.33 \pm 0.02$ when the buoyancy source is homogeneous, $R_\rho = 1$. The influence of the density difference ratio and the buoyancy distribution parameter on the Froude number in the inertial phase is best illustrated in Fig. 15. For gravity currents produced from nonhomogeneous two-layer density-stratified buoyancy sources, the Froude number in the inertial phase is always less than that from a homogeneous source. When the buoyancy distribution parameter is maintained constant, it is found that the Froude number in the inertial phase decreases monotonically as the density difference ratio decreases. When the density difference ratio is maintained constant, it is found that the Froude number in the inertial phase has a local minimum value as the buoyancy distribution parameter falls in the range $0.3 \lesssim R_B \lesssim 0.5$. Interestingly, the initial potential energy, defined by (5) and listed in Table I, likewise shows a local minimum as the Froude number in the
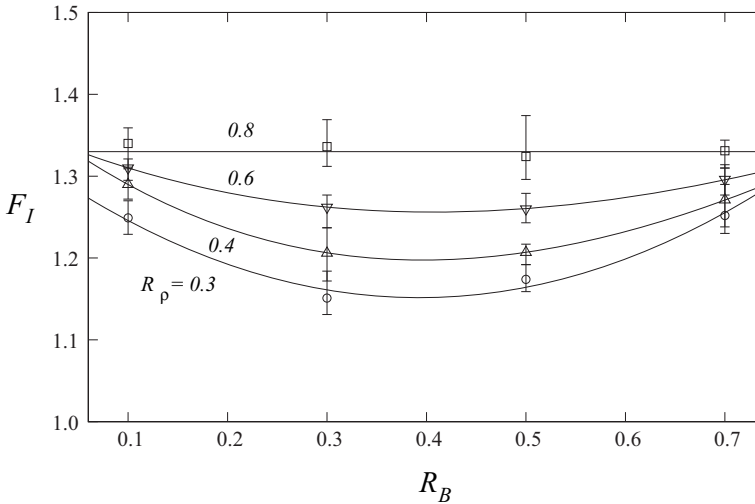
FIG. 15. Froude number in the inertial phase, F_I, against the buoyancy distribution parameter, R_B, at four different density difference ratios, $R_\rho = 0.3, 0.4, 0.6, 0.8$. Symbols: $\circ$, $R_\rho = 0.3$; $\triangle$, $R_\rho = 0.4$; $\triangledown$, $R_\rho = 0.6$; $\square$, $R_\rho = 0.8$. Solid lines represent the interpolating polynomials which describe the relationships between F_I and R_B at four different density difference ratios. The horizontal line, which is the best fit for $R_\rho = 0.8$, represents $F_I = 1.33$.

inertial phase does. It is then not unreasonable to speculate that the Froude number in the inertial phase in the problem under investigation is dictated by the initial potential energy in the two-layer system. The discernible difference in the Froude number between Ref. [47] and the present study may be attributed to the insufficient temporal resolution and the way Froude number was computed in Ref. [47]. In Ref. [47], photographs were taken every 4 s and the Frouder number was computed every 4 s based on the calculated front velocity and (6). In the present study, the temporal resolution is greatly improved and the Froude number is computed based on (7) without using the front velocity. Therefore, the dependence of Froude number on the controlling parameters, which was somewhat obscured in Ref. [47], is now made clear.

In geological environments, the buoyancy source is oftentimes composed of suspended particles of different sizes and the deposits of the particles are of particular interest. The two-layer density-stratified gravity currents serve as the least complicated model for a better understanding of the characteristics of the deposits made by stratified, particulate gravity currents, since in particulate gravity currents, coarse particles settle towards the lower layer while the fine particles remain in the upper layer. For a homogeneous and a weakly stratified, particulate buoyancy source, it is likely that well-mixed deposits will form as the flow propagates. For a strongly stratified, particulate buoyancy source, different forms of deposits may occur depending on the distribution of buoyancy between the two layers. When the lower layer dominates, $R_B \to 0$, coarse particles will be transported farther away from the source than the fine particles, and the deposits of coarse particles and deposits of fine particles may separate along the flow path. When the upper layer dominates, $R_B \to 1$, the fine particles can be transported farther and possibly overlain by sparse coarse particles. When the buoyancy distribution parameter falls in the range of $0.3 \lesssim R_B \lesssim 0.5$, the deposits of fine particles can be led by more well-mixed deposits of both coarse and fine particles. We should keep in mind that such an implication is based on the notion that the lower and upper layers in the experiments are proxies for the layers containing the coarse and fine particles, respectively, and the change in buoyancy, possibly due to particle settling from the flow and particle resuspension from the bed, is not considered in the simple model. Should these additional factors come into play, transition from one type of flow morphology into another is likely to occur as the flow evolves since the density contrast and the buoyancy distribution between the layers may change as the gravity currents propagate.

[1] J. Allen, *Principles of Physical Sedimentology* (Allen & Unwin, London, 1985).

[2] T. K. Fannelop, *Fluid Mechanics for Industrial Safety and Environmental Protection* (Elsevier, 1994).

[3] J. Simpson, *Gravity Currents*, 2nd ed. (Cambridge University Press, 1997).

[4] M. Ungarish, *An Introduction to Gravity Currents and Intrusions* (Chapman & Hall/CRC Press, 2009).

[5] J. Shin, S. Dalziel, and P. F. Linden, Gravity currents produced by lock exchange, J. Fluid Mech. **521**, 1 (2004).

[6] B. Marino, L. Thomas, and P. F. Linden, The front condition for gravity currents, J. Fluid Mech. **536**, 49 (2005).

[7] M. Cantero, J. Lee, S. Balachandar, and M. Garcia, On the front velocity of gravity currents, J. Fluid Mech. **586**, 1 (2007).

[8] M. L. Rocca, C. Adduce, G. Sciortino, and A. B. Pinzon, Experimental and numerical simulation of three-dimensional gravity currents on smooth and rough bottom, Phys. Fluids **20**, 106603 (2008).

[9] M. L. Rocca, C. Adduce, V. Lombardi, G. Sciortino, and R. Hinkermann, Development of a lattice Boltzmann method for two-layered shallow-water flow, Int. J. Numer. Methods Fluids **70**, 1048 (2012).

[10] M. L. Rocca, C. Adduce, G. Sciortino, P. A. Bateman, and M. A. Boniforti, A two-layer shallow water model for 3D gravity currents, J. Hydraul. Res. **50**, 208 (2012).

[11] C. Adduce, G. Sciortino, and S. Proietti, Gravity currents produced by lock-exchanges: Experiments and simulations with a two layer shallow-water model with entrainment, J. Hydraul. Eng. **138**, 111 (2012).

[12] L. Ottolenghi, C. Adduce, R. Inghilesi, V. Armenio, and F. Roman, Entrainment and mixing in unsteady gravity currents, J. Hydraul. Res. **54**, 541 (2016).

[13] M. Ungarish, C. A. Mériaux, and C. B. Kurz-Besson, The propagation of gravity currents in a V-shaped triangular cross-section channel: Experiments and theory, J. Fluid Mech. **754**, 232 (2014).

[14] T. Maxworthy and R. I. Nokes, Experiments on gravity currents propagating down slopes. Part 1. The release of a fixed volume of heavy fluid from an enclosed lock into an open channel, J. Fluid Mech. **584**, 433 (2007).

[15] T. Maxworthy, Experiments on gravity currents propagating down slopes. Part 2. The evolution of a fixed volume of fluid released from closed locks into a long, open channel, J. Fluid Mech. **647**, 27 (2010).

[16] A. Dai, Experiments on gravity currents propagating on different bottom slopes, J. Fluid Mech. **731**, 117 (2013).

[17] A. Dai, Non-Boussinesq gravity currents propagating on different bottom slopes, J. Fluid Mech. **741**, 658 (2014).

[18] A. Dai, High-resolution simulations of downslope gravity currents in the acceleration phase, Phys. Fluids **27**, 076602 (2015).

[19] A. Dai and Y.-L. Huang, High-resolution simulations of non-Boussinesq downslope gravity currents in the acceleration phase, Phys. Fluids **28**, 026602 (2016).

[20] C. S. Jones, C. Cenedese, E. P. Chassignet, P. F. Linden, and B. R. Sutherland, Gravity current propagation up a valley, J. Fluid Mech. **762**, 417 (2014).

[21] L. J. Marleau, M. R. Flynn, and B. R. Sutherland, Gravity currents propagating up a slope, Phys. Fluids **26**, 046605 (2014).

[22] V. Lombardi, C. Adduce, G. Sciortino, and M. L. Rocca, Gravity currents flowing upslope: Laboratory experiments and shallow-water simulations, Phys. Fluids **27**, 016602 (2015).

[23] L. Ottolenghi, C. Adduce, R. Inghilesi, F. Roman, and V. Armenio, Mixing in lock-release gravity currents propagating up a slope, Phys. Fluids **28**, 056604 (2016).

[24] G. H. Keulegan, The motion of saline fronts in still water, Natl. Bur. Stand. Rep. 5813 (1958).

[25] D. I. H. Barr, Densimetric exchange flows in rectangular channels, Houille Blanche **22**, 619 (1967).

[26] T. B. Benjamin, Gravity currents and related phenomena, J. Fluid Mech. **31**, 209 (1968).

[27] H. E. Huppert and J. Simpson, The slumping of gravity currents, J. Fluid Mech. **99**, 785 (1980).

[28] H. E. Huppert, The propagation of two-dimensional and axisymmetric viscous gravity currents over a rigid horizontal boundary surface, J. Fluid Mech. **121**, 43 (1982).

[29] T. Maxworthy, J. Leilich, J. E. Simpson, and E. H. Meiburg, The propagation of a gravity current into a linearly stratified fluid, J. Fluid Mech. **453**, 371 (2002).

[30] M. Ungarish and H. E. Huppert, On gravity currents propagating at the base of a stratified ambient, J. Fluid Mech. **458**, 283 (2002).

[31] M. Ungarish and H. E. Huppert, On gravity currents propagating at the base of a stratified ambient: Effects of geometrical constraints and rotation, J. Fluid Mech. **521**, 69 (2004).

[32] M. Ungarish, On gravity currents in a linearly stratified ambient: A generalization of Benjamin's steady-state propagation results, J. Fluid Mech. **548**, 49 (2006).

[33] M. Ungarish and H. E. Huppert, Energy balances for propagating gravity currents: Homogeneous and stratified ambients, J. Fluid Mech. **565**, 363 (2006).

[34] V. K. Birman, E. Meiburg, and M. Ungarish, On gravity currents in stratified ambients, Phys. Fluids **19**, 086602 (2007).

[35] J. Wu, Mixed region collapse with internal wave generation in a density-stratified medium, J. Fluid Mech. **35**, 531 (1969).

[36] A. H. Schooley and B. A. Hughes, An experimental and theoretical study of internal waves generated by the collapse of a two-dimensional mixed region in a density gradient, J. Fluid Mech. **51**, 159 (1972).

[37] R. Amen and T. Maxworthy, The gravitational collapse of a mixed region into a linearly stratified fluid, J. Fluid Mech. **96**, 65 (1980).

[38] M. R. Flynn and B. R. Sutherland, Intrusive gravity currents and internal gravity wave generation in stratified fluid, J. Fluid Mech. **514**, 355 (2004).

[39] M. Ungarish, Intrusive gravity currents in a stratified ambient: Shallow-water theory and numerical results, J. Fluid Mech. **535**, 287 (2005).

[40] M. R. Flynn and P. F. Linden, Intrusive gravity currents, J. Fluid Mech. **568**, 193 (2006).

[41] B. D. Maurer, D. T. Bolster, and P. F. Linden, Intrusive gravity currents between two stably stratified fluids, J. Fluid Mech. **647**, 53 (2010).

[42] C. J. Clayton, Contrasting sediment gravity flow processes in the late Llandovery, Rhuddnant Grits turbidite system, Welsh Basin, J. Geol. **29**, 167 (1994).

[43] H. D. Sinclair, The influence of lateral basinal slopes on turbidite sedimentation in the Annot sandstones of SE France, J. Sed. Res. **64**, 42 (1994).

[44] I. N. McCave and K. P. N. Jones, Deposition of ungraded muds from high density non-turbulent turbidity currents, Nature (London) **333**, 250 (1988).

[45] C. M. Choux and T. H. Druitt, Analogue study of particle segregation in pyroclastic density currents, with implications for the emplacement mechanisms of large ignimbrites, Sedimentology **49**, 907 (2002).

[46] C. Gladstone and R. S. J. Sparks, The significance of grainsize breaks in turbidites and pyroclastic density current deposits, J. Sed. Res. **72**, 182 (2002).

[47] C. Gladstone, L. J. Ritchie, R. S. J. Sparks, and A. W. Woods, An experimental investigation of density-stratified inertial gravity currents, Sedimentology **51**, 767 (2004).

[48] J. S. Turner, *Buoyancy Effects in Fluids* (Cambridge University Press, 1979).

[49] T. H. Ellison and J. S. Turner, Turbulent entrainment in stratified flows, J. Fluid Mech. **6**, 423 (1959).

[50] M. Hallworth, H. E. Huppert, J. Phillips, and R. S. J. Sparks, Entrainment into two-dimensional and axisymmetric turbulent gravity currents, J. Fluid Mech. **308**, 289 (1996).

[51] J. D. Parsons and M. H. Garcia, Similarity of gravity current fronts, Phys. Fluids **10**, 3209 (1988).

[52] C. P. Caulfield and R. R. Kerswell, Maximal mixing rate in turbulent stratified Couette flow, Phys. Fluids **13**, 894 (2001).

[53] J. K. Venard and R. L. Street, *Elementary Fluid Mechanics*, 5th ed. (Wiley, New York, 1975).

[54] J. W. Rottman and J. E. Simpson, Gravity currents produced by instantaneous releases of a heavy fluid in a rectangular channel, J. Fluid Mech. **135**, 95 (1983).